HHS Public Access

Author manuscript

Acta Biomater. Author manuscript; available in PMC 2019 April 15.

Published in final edited form as:

Acta Biomater. 2018 April 15; 71: 1–23. doi:10.1016/j.actbio.2018.03.005.

Zinc-based alloys for degradable vascular stent applications

Ehsan Mostaed[a,b,1], **Malgorzata Sikora-Jasinska**[b,c], **Jaroslaw W. Drelich**[a], **Maurizio Vedani**[b]

[a]Department of Materials Science and Engineering, Michigan Technological University, Houghton, MI 49931, USA

[b]Department of Mechanical Engineering, Politecnico di Milano, Milan, Italy

[c]Laboratory for Biomaterials & Bioengineering (CRC-I), Department Min-Met-Materials Engineering & Research Center CHU de Québec, Laval University, Québec City, Canada

Abstract

The search for biodegradable metals with mechanical properties equal or higher to those of currently used permanent biomaterials, such as stainless steels, cobalt chromium and titanium alloys, desirable in vivo degradation rate and uniform corrosion is still an open challenge. Magnesium (Mg), iron (Fe) and zinc (Zn)-based alloys have been proposed as biodegradable metals for medical applications. Over the last two decades, extensive research has been done on Mg and Fe. Fe-based alloys show appropriate mechanical properties, but their degradation rate is an order of magnitude below the benchmark value. In comparison, alongside the insufficient mechanical performance of most of its alloys, Mg degradation rate has proven to be too high in a physiological environment and corrosion is rarely uniform. During the last few years, Zn alloys have been explored by the biomedical community as potential materials for bioabsorbable vascular stents due to their tolerable corrosion rates and tunable mechanical properties. This review summarizes recent progress made in developing Zn alloys for vascular stenting application. Novel Zn alloys are discussed regarding their microstructural characteristics, mechanical properties, corrosion behavior and *in vivo* performance.

Keywords

Bioabsorbable; Zinc alloys; Microstructure; Mechanical properties; Degradation

1. Introduction

Bioabsorbable metals are perceived as revolutionary biomedical materials and have been widely researched for both vascular and orthopedic applications over the last two decades. The concept of an absorbable stent is to keep the occluded arteries open during the remodeling period and degrade harmlessly afterward, when its mechanical scaffolding

[1]Corresponding author: Ehsan Mostaed, emostaed@mtu.edu.

support is no longer needed. As illustrated in Fig. 1a, a mesh tube stent, in its crimped state, is guided to an occluded artery using a balloon-tipped catheter. Once in place, the balloon is inflated to expand the stent diameter and push the plaque, opening the artery and restoring blood flow rate. The balloon is then deflated and removed while the stent remains in place and holds the artery open. Afterward, the arterial wall heals and remodels around the stent.

The stent material and its corrosion product must be non-toxic and compatible to the vascular environment. Hermawan et al. [1] described an ideal biodegradable stent as a device which should be able to compromise its mechanical integrity and be consumed by the host after its required service time, as per the qualitative trendline sketched in Fig. 1b. The authors argued that a slow corrosion, if any, is required in the first several weeks to preserve the optimal mechanical integrity of the stent. Then corrosion should progress with a similar rate as arterial vessel remodeling to allow for the healing process to complete. Afterward, the stent is supposed to disappear and leave behind a natural functioning artery. Previous studies reported that an ideal period of 6–12 months is expected for the remodeling of artery vessels [2,3].

The use of bioabsorbable stents drastically reduces, if not annihilates, some potentially long-term clinical problems related to permanent stents such as chronic inflammation, late stent thrombosis, in-stent restenosis and stent strut fracture. Additionally, in infants and children, once the stent disappears, the vessel is able to naturally grow until adulthood, eliminating the need for future surgery or stent balloon dilatation [4–6]. Thus, it is of great importance to develop a new generation of vascular stents which can degrade gradually enough to maintain their mechanical integrity during the period of arterial wall remodeling, and being completely and safely absorbed thereafter.

A degradable vascular stent material must fulfill the following clinical requirements [7,8]:

- Degrade at a rate of less than 0.02 mm/year,
- Have mechanical integrity for 3–6 months,
- Being bioabsorbed completely within 12–24 months, and
- Retain biocompatibility throughout implantation and degradation process (material must be non-toxic, non-inflammatory and should not generate harmful degradation products).

Additionally, the material must meet mechanical benchmark values as follows [7,9–11]:

- Young’s modulus should be as high as possible to prevent acute stent recoil after balloon deflation. The allowable elastic recoil of a stent on expansion should be below 4%;
- Yield strength to elastic modulus ratio, which provides an alternative criterion of expected recoil upon deflation of the balloon, should be in the range of 0.16–0.32;

- Reasonably low yield strength (YS) (200–300 MPa) is preferred to allow crimping of the stent onto a balloon tipped catheter and expansion of the stent at low balloon pressures during deployment in the intended location;
- High ultimate tensile strength (UTS) to increase stent radial strength and allow the design of thinner struts, thus improving flexibility and access to narrower vessels (> 300 MPa);
- A large work hardening rate, which leads to a favorable increase in strength during stent expansion and improves the fatigue life (expected at least 10 million cycles before complete dissolution);
- Adequate ductility to sustain deformation during expansion without cracking (at least 20% fracture elongation but some applications require this value to exceed 30%).

The aforementioned combination of mechanical properties in the same material is challenging, especially for zinc alloys. For instance, although, in most cases, higher UTS is associated with an increase in YS, it concurrently leads to a drop in ductility [12].

Over the last two decades, polymeric and metallic materials have been rigorously studied as candidates for degradable vascular stents. Polymeric stents, despite their predictable degradation products, identical degradation mechanisms *in vitro* and *in vivo* and acceptable biocompatibility, require a greater strut thickness than most metal stents due to their low radial strength [13,14]. Polymeric stents with thicker struts thus require larger catheters for delivery, which makes their use challenging in pediatric interventions. Polymers also exhibit poor visibility characteristics, thereby leading to lack of radiopacity for *in vivo* imaging [15]. Moreover, the inability to attain an acceptable permanent expansion along with susceptibility to restenosis are further concerns when using polymeric stents [7,16].

Metallic materials, especially those containing elements which are supplied in consistent quantities to boost human body metabolism, seem to be promising candidates for stent application owing to their easy translation to the clinical environment [17]. With enhanced mechanical strength and deformability such metals provide a platform for a variety of stent designs with a broad range of expandable diameters. To date, in the field of degradable metals, numerous studies on magnesium (Mg) and iron (Fe)-based alloys have been reported summarizing efforts on tailoring mechanical characteristics and corrosion behavior to address the requirements of bioabsorbable stent applications [1,7,12,17–20].

Mg has received a lot of attention as an attractive metallic material for stenting due to its excellent biocompatibility and low thrombogenicity [5]. Its recommended intake for adults lies between 240 and 400 mg/day [12,21,22], and Mg is not a source of concern for stenting application from toxicity point of view. However, its rapid degradation in physiological environments leads to early undermining of the stent’s mechanical integrity [21]. During the past several years, much research has been done to tailor the properties of Mg through alloying, advanced processing and surface modification techniques [19,23–26]. Research efforts have successfully resulted in the first clinically-proven resorbable Mg stent exhibiting nearly 95 % resorption within 12 months [27]. However, further improvements are still

needed to fully meet all the expected requirements identified for an ideal Mg-based stent material [7,17].

Fe is an essential trace element for the human body with a recommended intake of between 8 and 18 mg/day for adults [28]. In 2001, for the first time a study was carried out by Peuster et al. [29] on Fe as a potential bioabsorbable stent material. An Fe stent was implanted in the descending aorta of New Zealand white rabbits. The authors found no long-term restenosis and inflammatory response in blood vessels, which are common problems for permanent stents. Another study conducted by Waskman et al. [30] revealed no excessive formation of neointima. Fe and its alloys possess high radial strength, allowing the use of stents with substantially thinner struts and thereby reducing the restenosis rate. Moreover, their high ductility facilitates stent delivery through catheter-based systems. On the other hand, there are two main concerns regarding the use of Fe as a degradable stent material. First, it cannot be fully degraded over its expected service period of up to two years, leaving a large portion of the stent intact even one year after implantation [31]. More importantly, upon degradation it produces a relatively large volume of iron oxide products which might not be safely metabolized in the body [20]. Despite several attempts made over nearly two decades to accelerate the degradation of Fe through alloying with essential elements and/or low content of toxic elements, novel thermal treatments, processing and manufacturing routes including powder metallurgy and advanced forming techniques, further efforts are still required before Fe-based stents can progress to clinical trials [32,33].

In recent years, research has shifted towards Zn-based biodegradable materials due to promising biodegradability and adaptability to tissue regeneration. Zinc has a standard corrosion potential of −0.76V, which is intermediate between Fe (−0.44V) and Mg (−2.37V). Zn is an essential element in human nutrition and is the second most abundant transition metal element in the human body, playing a crucial role in cell proliferation as well as in the immune and nervous systems [34,35]. Moreover, Zn serves as a cofactor in all six classes of enzymes, as well as in several classes of regulatory proteins [34,36]. The recommended daily value of Zn starts from 2–3 mg/day for infants up to 8–11 mg/day for adults [28,34]. Zn also supports normal growth, wound healing and a proper sense of taste and smell [37]. Despite a lower toxicity limit for Zn (100–150 mg/day) than for Mg (375–500 mg/day), the toxicity threshold for Zn as a stent material is not a limitation because of the remarkably small volume of a stent (weight of about 50 mg to be dissolved in a target period of 12 months) [8,12]. Moreover, alongside its good biocompatibility in blood vessels and the appropriate degradation rate, Zn has a low melting point (420°C) and low reactivity in the molten state (unlike Mg), permitting melting and hot processing in air [38].

In 2013, a landmark report was published by Bowen et al. [8], who introduced Zn as an outstanding candidate for stent application. Pure Zn wires were implanted into the abdominal aorta of adult male Sprague-Dawley rats for up to 6 months. It was found that in the first 3 months Zn exhibited a uniform corrosion mode, while after 4.5 and 6 months *in vivo*, relatively severe and localized corrosion was observed. In more recent studies, it was reported that zinc wires implanted in the murine artery exhibit relatively steady corrosion, with a penetration rate of 0.25 ± 0.10 mm/y, without local toxicity for up to at least 20

months post-implantation [39] (Fig.2). This steady corrosion, if confirmed with additional in vivo studies, could simplify stent design in terms of their lifetime and corrosion progression.

This report reviews the most recent Zn-based alloys developed for medical applications, with the main focus being on alloy design/development, mechanical properties, corrosion behavior and in vivo assessments in a vascular environment. It complements the content of the first review on Zn-based biomaterials published in 2016 [7], offering analysis of novel alloys developed mainly in the last 2–3 years. At the time of preparation of the first review, research activities with Zn-based biomaterials were practically limited to 2–3 laboratories. The increased number of scientific reports on Zn implant materials since 2015 implies that this class of materials has become a point of investigation in various research laboratories across the world, working on biodegradable metals for medical applications. Although this review covers only vascular scaffolding applications, uses for Zn implants have also recently been explored in orthopedic, wound closure and drug-delivery applications, but these new applications are not covered in this review. Recent research also includes advances made in surface finish of zinc implants [40,41], but this topic is also not covered in this review.

2. Zinc alloy candidates for stenting applications

It is essential that an ideal biodegradable stent material has an appropriate degradation and in-service mechanical performance as well as an excellent biocompatibility. Despite fulfilling the degradation and biocompatibility requirements, the major concern of using pure Zn for stent manufacturing is its poor mechanical strength. The ultimate tensile strength (UTS) of Zn is only about 20 MPa and 120 MPa in cast and wrought conditions, respectively [42,43]. These values are far below the benchmark value required for a vascular stent material (UTS of about 300 MPa). Fortunately, compared to Mg, the intrinsic lower corrosion rate of Zn provides more freedom for metallurgical manipulation through alloying with a wide range of non-toxic elements that can be added in a wide range of quantities. In addition to alloying, grain refinement induced by thermomechanical treatments can further improve the mechanical characteristics of cast Zn alloys [43–45]. Existing Zn alloys, which are most commonly used in die casting, contain large amounts of A1, which is considered as a potentially toxic element by the FDA [46], (e.g. ZA8, ZA12 and ZA27 with 8–27 wt% aluminum, 1–3 wt% copper), and are therefore not considered at present for bio-applications. Therefore, knowledge-based designs of new Zn alloys have been initiated a few years ago, and both the effects of alloying elements and fabrication history on the degradation behavior and biocompatibility of Zn alloys are under extensive investigations. Apart from the mechanical point of view, when designing a Zn alloy for vascular stents, tailoring the degradation and maintaining, or even improving, the biocompatibility of the alloy are important factors to be considered. Hence, understanding the corrosion mechanism and its effect on the biocompatibility of Zn alloys is a precondition for the development of biodegradable Zn stent alloys.

Only a limited number of Zn alloy systems have been investigated as potential biodegradable materials thus far [43,44,47–55]. Since Mg, Ca, Sr and Mn are reported as essential elements for the human body [56,57], they should be the first choice as alloying elements for biomedical Zn alloys. Elements with potential toxicological problems must preferably be

avoided in the initial design stage for biodegradable alloys or used at a concentration that is acceptable to the host body. The degradation products of the alloys should also be non-toxic and readily absorbable by the surrounding tissues. The following is a brief review of Zn alloys, which were formulated and characterized.

2.1. Zn-based alloy systems for biomedical applications

2.1.1. Zn-Mg alloy system

2.1.1.1. Microstructure and mechanical properties: As a well-explored biocompatible metal, Mg is an evident choice of alloying element for Zn. Zn-Mg binary alloys are expected to have superior mechanical properties while maintaining high biosafety. According to the Zn-Mg phase diagram shown in Fig. 3, the maximum solubility of Mg in Zn is about 0.1 wt. % at 364°C.

Mostaed et al. [43] formulated a series of Zn-Mg binary alloys with Mg contents ranging from 0.15 to 3.0 wt.%. As depicted in Fig. 4a to 4c, they revealed that below the eutectic composition (3.0 wt.% Mg) the microstructure of the alloys consisted of primary α-Zn dendritic grains along with a Zn + Mg_2Zn_{11} eutectic, mainly located at grain boundaries. Increasing the Mg content led to an increase in the volume fraction of the eutectic mixture and a decrease in the grain size of the alloys. Eventually, a fully eutectic structure with fine alternate lamellae of Zn and Mg_2Zn_{11} (Fig. 4d) was obtained in the Zn–3.0Mg alloy.

Similarly, Vojtech et al. [42] investigated the mechanical properties of as-cast Zn-Mg alloys, but for orthopedic applications. They found that adding 1wt.% Mg markedly improves the mechanical strength of Zn, from 20 MPa to about 190 MPa through the formation of a Zn +Mg_2Zn_{11} eutectic mixture, while the elongation-to-failure value decreased below 2%. These properties are not sufficient for many load-bearing applications in biodegradable devices. Similar mechanical properties of as-cast Zn-1.2 wt.% Mg with YS, UTS and fracture elongation of 117 MPa, 130 MPa and 1.4%, respectively, were also reported by Shen et al. [45]. Mg content of ~ 1wt.% and above gives rise to an increase in the volume fraction of the brittle eutectic and, therefore, deterioration in alloy ductility and fracture toughness. Hence, for vascular stents, properties of Zn-Mg alloys must be improved through either addition of other alloying elements or applying post-treatments.

The addition of nutrient elements like calcium (Ca), strontium (Sr) and other essential trace elements such as manganese (Mn) have recently been investigated as minor additions in some Zn alloys [51,54,58]. Liu et al. [54] reported that the addition of 0.1wt.% Sr and Ca to Zn-1.5Mg alloy improves tensile strength from 151 MPa to 209 MPa and 241 MPa, respectively, but fracture elongation was still below 2%.

Ductility limitations of cast structures can substantially be removed by post-solidification thermomechanical treatments. Li et al. [51] showed significantly improved tensile strength and ductility of Zn-1.0Mg alloy from 130 MPa and 1% to 298 MPa and 26%, respectively, through a combination of micro alloying with Mn (0.1 wt.%) and hot rolling. Mostaed et.al [43] demonstrated that hot extrusion of Zn-Mg alloys produces a fine equiaxed grain structure made by a mixture of Zn and Mg_2Zn_{11} particles, which were distributed along the extrusion direction in a non-uniform manner (Fig. 5). It was also found that hot extrusion

could not successfully break the Mg_2Zn_{11} phase, giving a rather wide range of particle sizes (1–20 μm). They showed that an increase in the Mg content up to 0.5 wt.% leads to both grain refinement and increased volume fraction of the hard Mg_2Zn_{11} intermetallic phase, improving the combination of mechanical properties. It was also reported that the Zn-0.5Mg alloy could achieve the best compromise for stent application (UTS = 297 MPa and fracture elongation of 13%).

However, in any Zn-Mg alloy containing coarse Mg_2Zn_{11} particles, micro-cracks can be initiated at the Zn/Mg_2Zn_{11} interface when the alloy undergoes subsequent cold work processing due to the large mechanical mismatch between soft Zn matrix and brittle Mg_2Zn_{11} particles As cold working advances, the micro-cracks coalesce, which may result in premature failure. Fig. 6 shows the microstructure of a Zn-0.5Mg wire with internal cracks produced after 60% of cold work.

Two research groups have recently reported unusual behavior in Zn-Mg micro-alloys. Jin et al. [59] successfully drew Zn-0.002Mg, Zn-0.05Mg and Zn-0.08Mg alloy rods from an initial diameter of 10 mm to 0.25 mm (~ 99.9% of deformation) at room temperature. Although the tensile properties of the drawn wires in the same day of drawing were in the order of values reported by other studies [43,45,48,51,54,58], interestingly, after only one day the YS and UTS remarkably increased from 250 MPa and 266 MPa to 449 MPa and 483 MPa, respectively. Similarly, Zn-0.02Mg alloy was cold drawn up to a cumulative strain of 97% in another study carried out by Wang et al. [60]. As seen in Fig. 7, the researchers found that the extensive amount of cold work leads to the formation of significantly refined equiaxed grain structure separated by high angle grain boundaries (highlighted by black color) with an average grain size of about 1μm. This implies the occurrence of dynamic recrystallization in the mentioned alloy at room temperature. In their work, striking improvement of tensile strength from 167 MPa to 455 MPa (~ 170%) was reported. Unfortunately the storing time (the time between drawing and tensile testing) was not mentioned.

Based on the findings of Jin et al. [59] and Wang et al. [60] for Zn-Mg micro-alloys, it can be concluded that while an alloying element is in the solute form (solid solution Zn alloy) - similar to pure Zn with a very low recrystallization temperature of 10°C [61] - the Zn alloy could be recrystallized at room temperature, which allows an extensive amount of cold deformation without any failure. This results in a markedly refined microstructure with high density of grain boundaries, which are considered a high speed diffusion path for elements [61], accelerating the diffusion of solute atoms and thereby, precipitation of secondary phases at room temperature. Although Wang et al. [60] declared that the tensile strength enhancement was due to the grain refinement (25 μm vs 1 μm, for as-extruded and cold drawn wires, respectively), findings by Jin et al. [59] suggest that the main strengthening mechanism in Zn-Mg microalloys is room temperature shelf aging at which extremely fine Mg_2Zn_{11} particles precipitate at grain boundaries. Therefore, solid solution Zn-Mg binary alloys are strongly dependent on room temperature age hardening, resulting in mechanical properties instability. Age hardening of Zn-Mg alloys is a poorly understood phenomenon and requires intensive investigation. It should also be noted that such instability has not yet

been reported for other Zn-based alloys and thus, it is of paramount importance to be addressed in the future.

2.1.1.2. Corrosion and bioresorption: Several researchers investigated the corrosion behavior of Zn-Mg binary alloys for biodegradable implant applications [42,43,45,62]. Gong et al. [62] studied the corrosion behavior of Zn-1Mg alloys in as cast and extruded conditions. In their work, hot extrusion was found to be beneficial in hindering non-uniform micro-galvanic corrosion of Zn-Mg alloys. The extrusion process resulted in general homogenization of the chemical composition and distribution of constituents by grain refinement and recrystallization. Large precipitates were broken down into finer particles and uniformly spread throughout the metallic matrix. This finding is consistent with the corrosion mechanism for as-cast and extruded Zn-xMg binary alloys (X=0.5, 1, 3%) proposed by Mostaed et al. [43].

The formation of magnesium hydroxyl carbonate was reported for Mg containing Zn alloys:

$$2Mg^{2+} + 2OH^{-} + CO_2^{2-} \rightarrow Mg_2(OH)_2CO_3 \quad (12)$$

Moreover, it was suggested that Mg may improve the corrosion resistance of Zn-based alloys by the formation of electrochemically inert compounds such as $Mg_2(OH)_2CO_3$ on the surface of investigated specimens. A Mg-containing form of simonkolleite has been reported to act as a corrosion barrier [63].

Corrosion rates calculated for Zn-Mg alloys differed from each other. Hot rolled Zn-1Mg alloy exhibited a corrosion rate of about 0.085 mm/year [48]. This is very close to the value calculated by Jablonská et al. (0.0134 $mg \cdot cm^{-2} \cdot day^{-1}$ which corresponds to 0.071 $mm \cdot year^{-1}$) [64]. Gong et al. [62] reported corrosion rates of 0.12 $mm \cdot year^{-1}$ for extruded Zn-1Mg. The reason for this higher corrosion rate compared with the other results could be related to the high amount of eutectic constituent found in the microstructure of their alloy, causing severe dissolution of the alloy's matrix [62]. The corrosion rates of various Zn-Mg alloys and their testing conditions are summarized in Table 1. The listed data reveals that corrosion rates estimated by weight changes and by electrochemistry can be significantly different.

Liu et al. [51,54] proposed ternary alloys with Mg content up to 1.5 wt.% alloyed with 0.5 wt.% Mn, Ca or Sr. The measured corrosion rates of these ternary alloys were slightly higher (Table 1) due to galvanic interaction between various phases formed during processing of these materials, including Mg_2Zn_{11} and $CaZn_{13}$ for Zn–1.5Mg–0.1Ca alloy, Mg_2Zn_{11}, and $SrZn_{13}$ for Zn–1.5Mg–0.1Sr..

Wang et al. [65] performed corrosion tests on Zn-Mg-Fe drawn and rolled mini-tubes. The drawn Zn alloy mini-tubes exhibited a rapid increase in weight loss during the first few days but corrosion rate stabilized after that. Furthermore, from the beginning to the end of the 48^{th} day of the immersion tests, weight loss for Zn drawn mini-tubes was observed to be higher than for their rolled counterpart, which was attributed to micro-defects introduced on the drawn tube surfaces.

2.1.2. Zn-Ca/Sr alloy systems

2.1.2.1. Microstructure and mechanical properties: Ca and Sr are well-known essential nutrient elements, constituting major components of bone tissue. Ca reaches a level of 0.919–0.993 $mg.L^{-1}$ in normal blood serum. The recommended Ca dietary allowance for adults is approximately 1g per day [66]. It is the most abundant mineral in the body, existing primarily in the skeleton where it serves as a body frame and as a reserve when dietary calcium is not sufficient. Sr is known as an osteopromotive element which can activate osteoblastic cell replication and decrease bone resorption while stimulating bone formation [67,68]. The distribution of Sr is similar to Ca. The human body contains about 320 mg strontium, approximately 99% of which is stored in the skeleton, preferably in new trabecular bone as a Ca substitute in hydroxyapatite [67]. Hence, Ca and Sr are attractive alloying elements for an orthopedic biodegradable implant material [69].

As per phase diagram in Fig. 8, Ca and Sr have no solubility in Zn and even in dilute Zn alloy systems they react with Zn, leading to the formation of $CaZn_{13}$ and $SrZn_{13}$ intermetallic compounds. Ca and Sr are alkali metals belonging to the second group in the periodic table. As of today, the only report on Zn-Ca and Zn-Sr alloy systems has been published by Li et al. [48] who developed Zn-1.0Ca and Zn-1.0Sr alloys to use as potential biodegradable materials within bone. Unfortunately, since the microstructures of these alloys have not been indicated in that report, information regarding the grain size, secondary phase size/morphology and distribution are not available. They further employed two hot working routes (rolling and extrusion) to improve the mechanical performance of the investigated alloys. It was found that hot worked Zn-1.0Ca and Zn-1.0Sr alloys exhibit nearly similar tensile strength (between 230–260 MPa), while the higher fracture elongation was always obtained for Zn-1.0Sr alloys (11% and 20% for extruded and rolled samples, respectively). However, compared to the benchmark values described in the previous section, such mechanical properties are still not sufficient to provide scaffolding support to the arterial wall during the remodeling period.

2.1.2.2. Corrosion and bioresorption: Li et al. [48] investigated the effect of Ca and Sr addition on the corrosion behavior of Zn-1.0Ca and Zn-1.0Sr alloys. They indicated that the corrosion rates measured by weight loss test using Hanks′ modified solution slightly increased from 0.08 to 0.09 and 0.95 mm/year for Zn to Zn-1.0Ca and Zn-1.0Sr, respectively. They also reported a similar increasing trend of corrosion rate measured by potentiodynamic polarization test. Another study conducted by the same group revealed that concurrent addition of Ca and Sr could further enhance the corrosion rate from 0.09 to 0.11 mm/year for Zn-1.0Ca and Zn-1.0Ca-1.0Sr, respectively [55]. However, no information about the corrosion mechanism and corrosion morphology/products was reported.

2.1.3. Zn-Al alloy system

2.1.3.1. Microstructure and Mechanical properties: Al is recognized as a neurotoxin which causes cognitive deficiency. The link between Al and increased risk of developing Alzheimer’s disease has been the subject of scientific debate for several decades. It was reported that the human body receives Al at a daily level of 1–10 mg from natural sources [70]. Kawahara suggested that for an average person, the recommended daily intake of Al is

about 10 mg [71]. Therefore, as reported by Bowen et al. [49], considering a potential Zn-Al alloy stent weighting about 50 mg and assuming that its complete degradation requires 12 months, the absorbed daily dose of Al would be far below the recommended value for humans (e.g. 0.006 mg for a 5 wt.% Al-containing Zn alloy).

As mentioned in Introduction, Al is the most commonly used alloying element in current Zn alloys available on the market. Zn-Al alloys are also the most documented Zn alloys in literature and they are designed for inexpensive structural and decorative parts in automotive, electronics and household sectors [72]. Copper and magnesium elements are added into Zn-Al alloys as well, to further improve mechanical and corrosion performances [73].

As seen in Fig. 9, at 5 wt.% Al and 381°C, Zn-Al alloy undergoes an eutectic transformation forming β-Zn (hexagonal close packed crystal) solid solution with a maximum solubility of 1.2 wt.% Al along with α′-Al rich (cubic face centered crystal) solid solution. As the cooling advances, at 277°C and 22 wt.% Al, the α′ phase experiences a monotectoid transformation through which a lamellar constituent consisting of α-phase with lower Zn content, and β-phase solid solution forms.

The properties of low Al-bearing extruded Zn alloys containing 0.5 and 1wt.% Al have been investigated by Mostaed et al. [43] and compared to their Mg-bearing alloy counterparts. Fig. 10a shows the microstructure of Zn-1.0Al alloy in as-cast condition, consisting of β-Zn dendrites accompanied by the interdendritic α+β constituents. They demonstrated that by solution heat treatment, the α+β mixture could be dissolved in the β-Zn matrix, forming a supersaturated β-Zn solid solution. Fig. 10b shows the microstructure of the Zn-1.0Al alloy after solution treatment and hot extrusion at 250°C. As seen, an equiaxial grain structure confirms the occurrence of significant grain refinement even after hot extrusion. Unlike the Zn-Mg alloys investigated in the same report, no second phase particles were found (Fig. 10b vs Fig. 5), which is consistent with the higher Al solubility in β-Zn. They also found that Al has a smaller effect on mechanical properties than Mg, since the formed single-phase structure is more prone to grain coarsening.

Bowen et al. [49] reported recently the properties of several wrought Zn-*x*Al alloys (*x*=1–5 wt.%) for stent applications. They indicated a UTS value of 245 MPa, slightly higher than that reported by Mostaed et al. [43] (223 MPa) for Zn-1.0Al alloy, while having an identical elongation to failure (~25%). Furthermore, they reported even higher UTS (308 MPa) and fracture elongation values (31 %) for Zn-5.0Al and Zn-3.0Al, respectively.

As noted before, as an alloying element in a tiny stent with a relatively long degradation time, Al will likely not cause any hazardous effects. Mechanical properties of Zn-Al alloys might be further improved through addition of alternative nutrient elements such as Mg, Ca and Sr into Zn-Al alloys having low Al content. Fig. 11 depicts the microstructure of air cooled cast Zn-1.0Al-1.0Mg alloy. The Zn + Mg_2Zn_{11} eutectic and β (Zn) + (α) Al monotectoid constituents are indicated by white and red arrows, respectively. Due to the higher solubility of Al in Zn, the volume fraction of the β + α microconstituent is remarkably lower than the lamellar Zn + Mg_2Zn_{11} eutectic mixture. Bakhsheshi-Rad et al.

[52] reported an increase in YS of cast Zn-0.5Al alloy from 79 MPa to 102 MPa with an addition of 0.5 wt.% Mg.

2.1.3.2. Corrosion and bioresorption: Bakhsheshi-Rad et al. fabricated binary, ternary (Zn-Al-Mg) [52] and quaternary (Zn-Al-Mg-Bi) [74] Zn-Al based alloys. Their results revealed that the quaternary Zn–Al–Mg–Bi alloys have a slightly lower corrosion resistance than those of the ternary Zn–Al–Mg and binary Zn-Al alloys. The main reason for the faster corrosion of Zn-Al–Mg–Bi than ternary Zn–Al–Mg was credited to the formation of a secondary phase (α-Mg_3Bi_2) which causes more extensive galvanic corrosion with the Zn based solid solution.

Wang et al. [75] evaluated the feasibility of commercial Zn-Al based alloys as biodegradable metals. In this work three commercial Zn alloys (ZA4-1, ZA4-3, ZA6-1) were prepared by hot extrusion at 200°C. It was confirmed that the galvanic corrosion formed between Zn matrix and α-Al increased the corrosion rates of pure Zn in Hanks' solution.

In a study conducted by Bowen et al. [49] the corrosion behavior of Zn-Al alloys was investigated in the murine aorta. They found that Zn-Al alloys undergo an intergranular corrosion which is distinctly different from that observed for pure Zn and other Zn alloys studied so far. The corrosion proceeds primarily by Al rich precipitates distributed at the grain boundaries which act as microanodic sites relative to the Zn matrix. They indicated that intergranular corrosion embrittles the alloy in the arterial environment, promoting microscale propagation of cracks and fragmentation of Zn-Al alloy implants.

2.1.4. Zn-Li alloy system

2.1.4.1. Microstructure and mechanical properties: The overdose of lithium (Li) may induce several potential health risks. Several researchers have reported that Li overdose causes congenital defects, especially of the cardiovascular system such as Ebstein's anomaly, when given to women during the first trimester of pregnancy [76]. Moreover, Aral et al. [77] investigated the toxicity of Li to humans. They reported that 10 mg L^{-1} Li in serum induces bipolar disorder, and at concentrations 20 mg L^{-1} and higher, there is a risk of death. However, Li is reported to be beneficial in several treatments such as brain injury, stroke, Alzheimer's, Huntington's and Parkinson's diseases and spinal cord injury, provided that it is kept below a critical content [78]. Based on clinical experiences, Li is nontoxic in the therapeutic range of 0.6–1.0 mM, while the toxic level occurs at 1.4 mM or higher [78].

As per phase diagram in Fig. 12, Li has a relatively low solubility in Zn (about 0.12 wt. % at 403°C) and therefore, under an equilibrium cooling condition, for any Li content above 0.12 wt% (within the eutectic range), Li has a tendency to form a lamellar Zn+$LiZn_4$ eutectic micro-constituent along the α-Zn grain boundaries.

Indeed, Li is an appealing element in a Mg alloy system due to its ability to change the lattice structure from hexagonal close-packed (HCP) into the body-centered cubic (BCC) crystal structure and, consequently, it markedly improves Mg ductility. For this reason, compared to other Mg alloys, Mg-Li alloys have a greater potential for meeting the

requirements for cardiovascular stents owing to their exceptional ductility and considerably low released dosage of Li from a tiny mesh tube [79,80].

Lithium was proposed as an alloying element to Zn by Zhao et al. [81]. According to the authors' estimation, for a Zn–Li alloy stent containing a relatively high Li content (1.7 wt.%), and considering a total degradation period of 1 year, the overall quantity of released Li is roughly two orders of magnitude below the daily body consumption allowance. Zhao et al. [81] designed, cast and hot rolled several binary Zn-*x*Li alloys (where *x*= 0.2, 0.4 and 0.7 wt.%, corresponding to hypoeutectic, eutectic and hypereutectic compositions, respectively), for use in biodegradable applications. It was found that, owing to the larger volume fraction of $LiZn_4$ intermetallic phase, an increase in Li addition from 0.2 wt.% to 0.7 wt.% results in a consistent enhancement of YS and UTS, from 240 MPa and 360 MPa to 480 MPa and 560 MPa, respectively. However, the measured ductility for the three alloys (14%, 14% and 2%, for Zn-0.2Li, Zn-0.4Li and Zn-0.7Li, respectively) is still fairly below the benchmark values (~ 20%) for stent materials.

2.1.4.2. Corrosion and bioresorption: An *in vitro* corrosion study on Zn-0.2Li and Zn-0.4Li alloys demonstrated that the corrosion rates and reaction products after immersion in modified SBF solution closely resemble those of pure Zn observed *in vivo*, in plasma, and in whole blood [81]. The Zn-0.4Li alloy exhibited higher resistance to corrosion compared to Zn-0.2Li, suggesting a positive effect of Li content on protective characteristics of the corrosion layer.

2.1.5. Zn-Ag alloy system

2.1.5.1. Microstructure and mechanical properties: Due to its strong antimicrobial properties, silver (Ag) has been applied by mankind for thousands of years. It maintains high antibacterial activity in a wide range of chemical states so that it effectively kills some superbugs which cannot be treated by most antibiotics [82]. Human use of silver has been described to be 0.4–27 μg/day [83]. Silver has been used for decades for burns and wound healing, being nowadays restored to many different medical applications [84,85]. Ag-containing materials have been successfully used as dental implants [86]. Some are introducing silver as a compound for biomaterial coatings [87]. Many studies, which have been performed based on Ag antibacterial properties, confirmed that silver ions or nanoparticles kill bacteria which adhere to the surface of an implant or prevent them from adhering to it [86,88]. It is worth noting that infection is one of the main concerns related to surgical implants, causing economic and clinical consequences since it postpones the healing process and in some cases leads to death. It is reported that the highest mortality related to the infection of surgical implants is registered among patients with cardiovascular stents [89]. Accordingly, adding Ag as an alloying element to Zn or Zn alloy systems would be of great interest for potential vascular stents.

Fig. 13 shows the Zn-Ag equilibrium phase diagram. At 431°C for an 8 wt.% Ag alloy, solidification occurs through a peritectic reaction in which a primary solid phase (β-$AgZn_3$) reacts with a liquid phase on cooling to produce a different solid phase (η-Zn solid solution). Peritectic reactions are commonly observed in systems with components that have large

melting point difference. Based on the phase diagram given in Fig. 13, Ag has a fairly high solubility in Zn and formation of any intermetallic phase, which leads to micro-galvanic corrosion, is prevented. Moreover, it would be possible to tailor the mechanical properties over a wide range by adjusting the Ag content in the solid solution. Accordingly, Zn-Ag might be a potentially suitable alloy system for vascular stent application.

Thus far, just one work has been published by Sikora-Jasinska et al. [44] on a Zn-Ag alloy system intended for biomedical applications. A new series of biodegradable Zn-Ag alloys with Ag content ranging from 2.5 to 7.0 wt.% were formulated. Fig. 14. depicts the microstructure of the as-cast and extruded Zn-7.0Ag alloy. The microstructure consists of primary η-Zn solid solution phase along with $AgZn_3$ dendrites. The $AgZn_3$ dendrites changed into fine precipitates (ranging from ~ 0.5–2 μm) distributed at the grain boundaries during the hot extrusion process. It was also found that after hot extrusion the microstructure of the alloys was significantly refined and the grain size decreased with increasing Ag content, giving a remarkably fine and equiaxed microstructure with a mean grain size of about 2 μm for the Zn-7.0Ag alloy. Among all Zn-based alloys which were explored by Sikora-Jasinska et al. [44], no microstructure with remarkably fine grains and ultra-fine/well distributed secondary phase particles have yet been reported. This finer microstructure not only markedly reduces micro galvanic coupling and thereby promotes uniform corrosion mode but also provides in a tiny vascular stent (strut thickness of about 100–160 μm) an enhanced number of grains occupying the strut section, thus remarkably improving the isotropic deformation behavior of the poly-crystal structure.

It was also confirmed that increasing the Ag content steadily enhanced the tensile strength from 203 MPa to 287 MPa for Zn-2.5Ag and Zn-7.0Ag, respectively, while, interestingly, the fracture elongation remained nearly unchanged (elongation to fracture in the range 32 to 36%), which is desirable for stenting applications [44]. In addition, among all designed alloys, Zn-7.0Ag displayed superplastic behavior over a wide range of strain rates. This creates the possibility of exploiting forming processes at fairly rapid rates and/or even at lower temperatures (maximum elongation of about 340 % and >400% was achieved at strain rates of 1.0×10^{-3} s^{-1} and 5.0×10^{-4} s^{-1}, respectively at a deformation temperature of 200°C).

2.1.5.2. Corrosion and bioresorption: Sikora-Jasinska et al. [44] studied the effect of Ag addition (2.5, 5.0 and 7.0 wt.%) on the degradation of Zn. The alloys with higher Ag content (5.0 and 7.0 wt.%) showed a trend toward more localized corrosion compared to the solid solution achieved in the Zn-2.5Ag alloy. This fact is attributed to the micro-galvanic effects caused by different potentials of the η-Zn solid solution and the $AgZn_3$ phases. Indeed, $AgZn_3$ particles act as sites for disruption of any oxide/hydroxide film covering the Zn-Ag alloys' surfaces. Recently, Torne et al. [90] carried out an investigation on the degradation mechanism of as-cast Zn-4.0Ag alloy in a Ringer's solution. Microstructural characterization on samples after 30 days of immersion showed selective corrosion surrounding $AgZn_3$ dendrites, leaving the $AgZn_3$ phase at the implant surface; nevertheless, no evident sign of corrosion pits was observed. Such enrichment of Ag at the interface may induce problematic cytotoxicity, affecting the tissue regeneration process. Thus, further investigation on biocompatibility of Ag-bearing Zn alloys could be of major significance at evaluating their competency as biodegradable implant materials.

2.1.6. Zn-Cu alloy system

2.1.6.1. Microstructure and mechanical properties: Copper (Cu) is an essential trace element necessary for development of connective tissues, nerve coverings and bone growth [91]. Cu promotes the proliferation of vascular endothelial cells, thus accelerating the revascularization process [92,93]. Cu deficiency causes normocytic anemia, neuropenia and abnormal glucose and cholesterol metabolism [94]. Cu deficiency also has adverse effects on the cardiovascular system such as atrial thrombosis, coronary necrosis and vascular calcification [94,95]. In an adult body, about 80 mg of Cu is found, mainly concentrated in liver and brain and the recommended dietary allowance for Cu is in the range of 2–3 mg/day [96]. Additionally, Cu ion is well recognized as having antimicrobial properties [97,98] and has been used as a sanitizing material and antimicrobial agent in toothpastes [99].

As shown in Fig. 15, Cu has a moderate solubility in Zn (2.75 wt.% Cu is soluble into Zn at 425°C). Similar to Zn-Ag system, Zn-Cu alloy experiences a peritectic reaction. Any Cu content between 2.7 wt.% to 22 wt.% results in the formation of a two-phase alloy consisting of primary ε-$CuZn_5$ dendrites and η-Zn solid solution.

Recently, Niu et al. [50] conducted research on Zn-4wt.%Cu alloy. They revealed that after extrusion, alongside refined microstructure promoted by the dynamic recrystallization, $CuZn_5$ dendrites were broken and distributed along the extrusion direction (bright particles in Fig. 16a), leading to enhanced mechanical performances (YS = 250 MPa and UTS = 270 MPa). Further research work carried out by the same group [100] suggested that the addition of Mg to Zn-Cu alloy systems could further enhance the tensile strength by the formation of an Mg_2Zn_{11} intermetallic phase (dark phase particles shown in Fig. 16). They also revealed that 1.0 wt.% addition of Mg to Zn-3.0Cu alloy increases the YS and UTS from 214 MPa and 250 MPa to 427 MPa and 440 MPa, respectively, while a drastic drop in elongation to failure, from 47% to 1%, was observed. Small differences between YS and UTS (which suggests a lack of work hardenability) for both Zn-Cu and Zn-Cu-Mg alloys, the poor ductility measured for the latter case, and the coarse and inhomogeneous distribution of intermetallic phases (as indicated in Fig. 16a and b) would make use of this alloy system for biodegradable applications quite challenging.

Lately, another study was conducted by the same group to study the effect of Fe addition on microstructure, mechanical and corrosion properties of Zn-3.0Cu-*x*Fe alloys (where x= 0.5 and 1 wt%) [101]. It was found that the addition of Fe did not contribute to microstructural uniformity. In particular, not only was no ternary intermetallic observed, but also, regardless of Fe content, a formation of coarse granular shaped $FeZn_{13}$ particles (20 μm–80 μm) coexisting with large $CuZn_5$ phase made the microstructure more non-uniform (Fig. 16c), and thus not favorable for degradable stent applications. Therefore, Fe addition did not enhance the tensile strength of the ternary Zn-Cu-Fe alloys. The authors reported that, instead, UTS values slightly decreased from 288 MPa for Zn-3.0Cu to 284 MPa and 272 MPa for Zn-3.0Cu-0.5Fe and Zn-3.0Cu-1.0Fe alloys, respectively. In contrast, the ductility of the investigated alloys was more influenced by Fe addition so that the fracture elongation markedly decreased from 46% to 33% and 20% for Zn-3.0Cu, Zn-3.0Cu-0.5Fe and Zn-3.0Cu-1.0Fe alloys, respectively. This was attributed to the propagation of extrusion-

induced cracks at the interface between soft Zn matrix (hardness of ~ 30 HV) and remarkably hard $FeZn_{13}$ particles (hardness of 270 HV) during the tensile testing which results in an early fracture.

2.1.6.2. Corrosion and bioresorption: Niu et al. [50] developed Zn-4.0Cu alloys with corrosion rate of 9.4 μm/year and uniform corrosion morphology without any evident galvanic coupling. Subsequently, Zn-3.0Cu alloys with addition of Mg or Fe up to 1 wt.% were developed by the same group [100,101]. It was found that the addition of Mg could increase corrosion rate of Zn-Cu alloys to 43 μm/year. The sharp increase in corrosion rate was attributed to the micro-galvanic corrosion effect between $FeZn_{13}$ particles and Zn matrix. Degradation rate of these alloys further increased to 68.8 μm/year [101].

2.1.7. Zn-Mn alloy system

2.1.7.1. Microstructure and mechanical properties: Manganese (Mn) is an essential trace element (<0.8 μg L^{-1} in blood serum) for the immune system and for a variety of enzymes [102]. Liu et al. [51] reported a very low hemolysis rate for rolled Zn–1Mg–0.1Mn alloy, confirming a good biocompatibility according to ASTM-F756-00. Moreover, they found no sign of thrombogenicity of the alloy with acceptable blood compatibility.

Mn has a rather low solubility in Zn (~ 0.8 wt.% at 405°C) (Fig. 17). Under equilibrium condition, at 1.2 wt.% Mn and at 405°C, Zn-Mn alloy experiences an eutectic transformation by which a Zn + $Zn_{13}Mn$ eutectic mixture forms. To date, the microstructure of as-cast Zn-Mn alloys has not been explored and, therefore, the morphology of Zn + $Zn_{13}Mn$ eutectic constituents has not been reported. Recently, Sun et al. [103] investigated the influence of Mn content on the mechanical performances of extruded Zn-Mn alloys. They revealed that unlike other Zn alloys reported heretofore, Mn has an inverse impact on the mechanical properties of Zn. Indeed, increasing the Mn content from 0.2 wt.% to 0.6 wt.% gave rise to a reduction of ultimate yield strength from 220 MPa to 182 MPa, while it considerably improved the fracture elongation, from 48% to 71%. They stated that such an effect, as depicted in Fig. 18, arises from the formation of tensile twining, mainly in dilute alloys, by which basal planes are rotated by 86.5° around the $\{10\bar{1}2\}$ axis. The volume fraction of the tensile twins in Zn-0.2Mn was measured to be 14.2%, while it decreased to 2.3% when 0.6 Mn was added. It was inferred that extension of twining had a key role in the mechanical properties of Zn-Mn alloys, acting as barriers to the movement of dislocations, and resulting in an increase in flow stress. Accordingly, Zn-0.2Mn alloy, despite having lower volume fraction of the $MnZn_{13}$ intermetallic, shows higher tensile strength than that of Zn-0.6Mn alloy.

2.1.7.2. Corrosion and bioresorption: Corrosion of Zn-Mn alloys has not been reported in literature yet.

2.2. Mechanical property degradation of Zn alloys

Adequate strength of biodegradable Zn implants is desirable during the healing process and is critical for postoperative rehabilitation. However, deterioration in mechanical integrity is expected as degradation progresses. Moreover, any mechanical load induced on the material

may accelerate this process due to the dual effect of corrosion and stress, leading to premature cracking. Unfortunately, very little was studied on changes in mechanical properties and fragmentation of Zn alloys.

Mostaed et al. [43] carried out compression tests on Zn, Zn-Mg and Zn-Al binary alloys before and after immersion in Hank's modified solution to evaluate the effect of corrosion on the material's mechanical properties. Compression specimens were immersed in Hanks' modified solution for two weeks. Results revealed up to a 20% drop in compressive yield strength for Zn-Mg alloys and this drop increased with increasing content of Mg from 0.15 to 1 wt.%. This effect was attributed to the increased volume fraction of the second phase, responsible for localized corrosion. In the same study, it was found that Zn-Al alloys have a slower loss of mechanical integrity, which was due to the presence of Al in the solute form, causing more homogenous corrosion mode. Li et al. [48] investigated the tensile properties of Zn-1Sr, Zn-1Ca and Zn-1Mg alloys for orthopedic applications after 2 and 8 weeks of immersion in Hanks' solution. Results revealed that alloys can retain their mechanical strength during the early implantation time.

2.3. Biological interactions

2.3.1. Cytotoxicity of Zn alloys—Although biodegradable metals are among the most innovative concepts introduced in the field of metallic biomaterials, their *in vitro* biocompatibility remains under-explored. As a result, there is only a small number of *in vitro* studies on the cytotoxicity of Zn ions (Table 2).

The rate of metal ion release from biodegradable alloys, such as Zn, Mg and Fe based materials, is significantly higher than that of permanent biomaterials. The released metallic ions may induce systemic toxicity to the human body as well as local toxicity to the peri-implant cells. Despite an outstanding biocompatibility of *in vivo* Zn-based implants, a rigorous understanding of how Zn and Zn^{2+} affect surrounding cells is missing. Protocols of current ISO standards (such as ISO 10993-5 or ISO 10993-12) do not apply to biodegradable metals and should be modified [104]. For example, Fischer et al. [105] recommended, in the case of Mg-based alloys, to use 10 times more extraction medium than recommended by the ISO standards to obtain reasonable results for reliable cytotoxicity evaluations of bioabsorbable Mg alloys *in vitro*. This recommendation might be suitable for Zn-based materials as well, although there is no clear guidelines. Consequently, researchers have applied different dilution levels of extracts while performing indirect cytotoxicity tests with Zn materials. In general, more diluted extracts (50% and below) contributed to increased biocompatibility [50,106,107]. A variety of cell lines has been used to evaluate the cytotoxicity of Zn alloys via *in vitro* experiments (Table 2). The choice of a specific cell type is of great importance for the performance of cytotoxicity tests and application of the investigated alloy.

Direct culture on metallic Zn revealed negligible cell survival despite Zn showing very good biocompatibility during *in vivo* tests [107]. This indicates the need to design a more representative *in vitro* experiment for cytotoxicity investigation of biodegradable metals. For example, Shearier at al. [107] modified the surface of Zn prior to direct culture on the metallic substrate. Collagen-based gelatin was deposited on Zn to mimic a protein layer *in*

vitro. Three human vascular cell types (endothelial, aortic smooth muscle, and dermal fibroblasts) used in this experiment could attach and proliferate on the modified Zn surface. Jablonska et al. [64] pre-incubated the Zn-1.5Mg alloy in SBF in order to create the protective surface layer, decreasing ion release and enhancing initial cell adhesion. Pre-incubation significantly decreased the corrosion rate of the alloy and increased metabolic activity of L929 after the indirect test. Moreover, it increased the number of U-2 OS cells adhered to the surface of the alloy in the direct test. Thus, surface pre-treatment prior to the cytotoxicity testing of biodegradable metallic materials can reduce the discrepancy between *in vitro* and *in vivo* results.

Ma et al. [108] studied the short-term cellular responses of human coronary artery endothelial cells (HCECs) under the influence of Zn^{2+} in concentrations up to 0.14 mM. They found that the cellular responses depend on the concentration of Zn^{2+} ions so that at low Zn^{2+} concentrations the cell viability, proliferation, adhesion, spreading and migration are enhanced, while it reduces the cell adhesion strength. In addition, low Zn^{2+} concentrations were found to have a significant effect on cell morphologies, changing them into an elongated-like shape. However, higher Zn^{2+} concentrations were reported to have a reverse effect on HCECs behavior.

Zhu et al. [109] assessed the biological responses of human bone marrow mesenchymal stem cells (hMSC) to pure Zn in comparison to AZ31 Mg alloy. They indicated that the density of viable cell adhesion on Zn was markedly higher than that on AZ31 alloy and remained almost unchanged over time. This was attributed to the fact that Zn absorbs more plasma proteins which facilitate cell adhesion. They reported considerably higher cell proliferation on Zn than that on AZ31 alloy during the first 14 days of culture. Moreover, they showed that Zn^{2+} stimulates intracellular signaling pathway in hMSC, which might enhance in vitro extracellular matrix (ECM) mineralization.

Murni et al. [110] evaluated a single concentration of Zn–3Mg alloy extract at 0.75mg/ml and its effect on the viability, performance in mineralization, and inflammatory reaction of NHOst cells. They reported a 30–50% decrease in cell viability when exposed to Zn-containing extracts, owing to the high concentration of Zn^{2+} in the extract (8μM). Moreover, the lower inhibitory effect of Zn–3Mg on the cells was ascribed to the presence of Mg as an alloying element which resulted in a lower corrosion rate than that of pure Zn.

2.3.2. *In vivo* testing of Zn-based biodegradable implants—Table 3 summarizes *in vivo* tests carried out on biodegradable Zn and Zn-based alloys. Using a murine preclinical model developed by Pierson et al. [20], wires made of pure Zn [8,39], Zn-Al [49], Zn-Mg [59] and Zn-Li [47] alloys were implanted into rat artery lumens to investigate biological responses of arterial environments to metals. These *in vivo* studies demonstrated that Zn and Zn alloys are well tolerated within rat abdominal aorta. In contrast to corrosion resistant metals that display a rigid and impenetrable interface to inflammatory cells, it was shown that Zn materials develop a dynamic interface that permits the penetration of inflammatory cells, phagocytic activity, and biomatrix regeneration. The degradation of Zn materials was found to be within the desired range of 0.02–0.03 mm/year with no chronic inflammatory response, localized necrosis or progressive intimal hyperplasia [8,39,111,112].

Additionally, local tissue response to the Zn implants revealed evidence of early tissue regeneration around the biocorrosion area, with no sign of local or systematic toxicity [112]. It was proven that the Zn implants could remain almost intact for the first 3–4 months of implantation due to the presence of a more corrosion resistant oxide film that always covers metallic zinc [40]. It was also shown that after a few months *in vivo,* the corrosion products were primarily benign compacted zinc oxides and zinc carbonate [112]. After partial degradation, tissue regenerated within the implant. More importantly, it was proven that Zn has an antiproliferative effect, preventing restenosis after stent implantation.

The *in vivo* studies at Michigan Tech also revealed marked differences in inflammatory response in rat arteries, attributed to the compositional dissimilarities of alloys that cause variations in implant corrosion behavior [111]. Zn–Al alloys exhibited an intergranular corrosion that is significantly different from that observed for pure Zn and other Zn alloys investigated so far [49]. There also appeared to be a trend of slightly worsening biocompatibility with increasing Mg content in zinc. As a result, the Zn-Mg alloys caused slightly elevated inflammation and neointimal activation as compared to what was observed for pure Zn [59]. It was speculated that Mg_2Zn_{11} particles promote a more aggressive activity of macrophages in an attempt to metabolize this alloy phase known for increased corrosion resistance. An enrichment of intermetallic particles in the corrosion product layer during in vivo degradation of zinc alloys and their effect on tissue regeneration is of concern [90] and has not been addressed yet.

The murine preclinical model [20] makes use of a single wire implant to simulate the presence of a stent strut within the vascular space. The application of radial force on the arterial wall with the potential for more extensive endothelial injury may result in different localized host tissue response to the material. Unfortunately, although a few in vivo studies with Zn stents using larger animals are under way, only one report was published so far. Yang et al. [113] implanted pure Zn stents into the abdominal aorta of rabbits for one year. Their findings coincide well with results of in vivo studies that involved Zn wires implanted into abdominal aorta of rats [39]. Specifically, the Zn stents biodegraded in about half after one year, with no severe signs of inflammation, intimal hyperplasia, and thrombosis formation. The researchers also observed healthy artery remodeling during stent degradation.

3. Discussion and comparative summery

3.1. Mechanical properties

Ultimate tensile strength (UTS) and elongation at fracture for various Zn-based alloys, in both as cast and wrought, are collected in Fig. 19. Cast alloys display a wide range of tensile strength, ranging from 70 MPa to 250 MPa, but with very poor ductility (<4%). The highest tensile strength was reported for Zn-1.5Mg-Ca/Sr alloys due to the combined strengthening contributions of brittle Zn + Mg_2Zn_{11} eutectic constituents and $CaZn_{13}$ and $SrZn_{13}$ intermetallic phases. However, the general mechanical performance, considered as the combination of strength and ductility, for all the reported cast Zn alloys listed in Fig. 19a is far below the benchmark values for vascular stent application (evaluated, as mentioned in the previous section, by values of tensile strength and fracture elongation exceeding 300 MPa

and 20%, respectively). Additional improvement in properties could be achieved by post thermomechanical treatments through tailoring microstructural features such as grain size, secondary phase size, their distribution and crystallographic texture.

Fig. 19b summarizes the tensile strength and fracture elongation of several wrought Zn-based alloys explored for biomedical applications during the last two years [42–45,48–52,54,55,58,81,100,101,114]. The red hachured region is where desirable materials with the desirable UTS and fracture elongation could be placed. However, by now, no Zn-based alloys have been introduced that fulfill the benchmark values required for an ideal absorbable stent material. For Mg bearing Zn alloys, which are the most investigated alloys (as represented with black legends in Fig. 19b), a parabolic trend can be seen so that with increasing Mg concentration UTS increases, while the elongation to failure decreases concurrently. However, it is apparent that any percentage of Mg higher than 0.5 wt% results in a drastic drop in fracture elongation. This trend is attributed to the increasing volume fraction of the brittle $MgZn_{11}$ intermetallic phase. In particular, it has been found that most elements added to Zn (e.g. Ca, Sr, Mg and Fe) form relatively coarse and sharp-edged intermetallics which promote crack initiation at the interface of matrix and particles either during hot forming or tensile testing. This has a detrimental influence on the ductility of Zn alloys. On the contrary, in the case of Zn-Ag alloys, increasing Ag content from 2.5 wt.% to 7.0 wt.% leads to a meaningful improvement in tensile strength and fracture elongation remains in the range of 32–36%. Ductility of these alloys was found to be not only attributed to the absence of any sharp-edged and coarse brittle intermetallics (see Fig.14b), but also to a high activity of the pyramidal <c+a> slip system. It should be noted that relative to the all binary and ternary Zn alloys, Zn-7.0Ag exhibits the best mechanical properties with a UTS and fracture elongation of 287 MPa and 32 %, respectively. Such an outstanding combination of high strength and ductility relies on the small grains, very fine and uniformly distributed precipitates and indeed favorable texture orientation for the <c+a> dislocation slip. However, among all the reported wrought alloys no materials seem to fully satisfy the mechanical benchmarks required for stent materials. Some alloys located in the grey hachured region of Fig. 19b are believed to be promising potential candidates for stent materials after further developments (Zn-0.15Mg, Zn-0.5Mg, Zn-3.0Cu, Zn-4.0Cu, Zn-5.0Ag, Zn-7.0Ag, Zn-5Al, Zn-0.4Li, Zn-0.7Li, Zn-3.0Cu-0.5Fe and Zn-3.0Cu-1.0Fe). It is expected that the mechanical properties of the mentioned alloys could be improved through composition modulation, microstructural optimization using thermal treatments (e.g. precipitation hardening), further grain/second phase refinement down to submicron regime and texture modification.

Opportunities to improve the mechanical properties and tune corrosion pattern of Zn alloys primarily lie in selection of alloying elements, their quantities and distribution in Zn matrix. Based on the information given in section 2.1.1, the alloying elements can be divided into three major groups: (i) elements with no or negligible solubility (Mg, Ca, Sr and Fe), (ii) elements of low or limited solubility (Al, Li and Cu) and (iii) elements of high solubility such as Ag. As of today, Zn systems alloyed with elements from the first two groups have been shown to be typically incapable of meeting the requirements for bioabsorbable stent materials due to the formation of relatively coarse and non-uniformly dispersed second phases. In these alloys the two main problems observed include:

- Poor ductility in cases of high alloying content or low strength when the alloying concentration is small;
- Early peak flow in the tensile curve, causing premature failure for a material like a stent which is under fatigue condition.

Employing advanced thermomechanical processing such as severe plastic deformation techniques, by which Mg alloys have been already successfully processed, might refine and redistribute the second phases and thereby, tailor the mechanical properties of these alloys. However, this approach has been poorly explored by the biomedical research community. In contrast, high-solubility elements provide the possibility to improve the mechanical properties of Zn through tuning the fraction/dispersion of the second phase particles within the matrix. Unfortunately, research with high-solubility elements has been limited to Ag.

3.2. Texture evaluation in wrought Zn alloys

As is well-documented in the literature [115,116], hexagonal close packed (hcp) metals and related alloys with c/a (where c is the elementary cell extension along hexagonal axis and a is the dimension along the hexagons) ratios close to the ideal value of 1.633 tend to form basal fiber textures during extrusion due to the high activity of basal slip systems. Fig. 20 shows the electron backscatter diffraction (EBSD) maps and their corresponding inverse pole figures obtained from the longitudinal section of ZK60 (Mg-5.3Zn–0.48Zr, wt.%) [117] and Zn-0.5Mg [43] alloys. For Mg (c/a =1.624) basal (0001) $<11\bar{2}0>$ slip results in a sharp basal fiber texture after extrusion, so that basal planes in the majority of the grains are distributed parallel to the extrusion direction (ED) (Fig. 20a). On the other hand, in Zn, unit cell which c/a exceeds the ideal value (c/a =1.856) due to the lower critical resolved shear stress (CRSS) of pyramidal $\{1\ 1\ \bar{2}\ \bar{2}\}\ <11\bar{2}3>$ than prismatic $\{1\ 0\ \bar{1}\ 0\}\ <11\bar{2}0>$ slip systems, a combination of basal and pyramidal slip leads to a texture with basal poles tilted toward ED. As seen in Fig. 20b, through the deformation process, the majority of recrystallized grains are tilted toward $[10\bar{1}0]$ and $[2\overline{11}0]$ poles after extrusion.

Such a developed texture in wrought Zn alloys results in higher Schmid factors for basal slip system than those of Mg alloy counterparts. The increase in Schmid factor values results in easy dislocation slip on the dominant slip plane (0002) and, thereby, lowers the stress required for yielding, which might improve the fracture elongation of the alloys in the case that the loading axis is parallel to the processing direction. Although texture has a crucial role in the mechanical properties of HCP metals (e.g. as important as grain size, if not superior, in Mg alloys), to date, no research has reported the effect of this parameter on the mechanical properties in Zn-based alloys. Thus, this would be of scientific interest to study the individual and combined effects of the grain size and texture on mechanical behavior of Zn alloys. Such studies could open new engineering routes in development of vascular Zn-based implants and complement the addition of alloying elements and applying thermomechanical processing, which have failed so far to produce Zn materials that meet the mechanical benchmarks for bioabsorbable vascular stents (see Fig. 19).

3.3. Degradation behavior

The Pourbaix diagram for Zn shows that in an acidic environment (i.e. urine), no surface oxides of Zn are stable, while under neutral or slightly alkaline conditions (i.e. blood plasma) zinc has the tendency to be passivated (Fig. 21) [118].

Pure Zn is a chemically reactive metal which dissolves in aqueous solutions through the following electrochemical reactions [119]:

$$Zn + OH^- = Zn(OH)_{ads.} + e \quad (1)$$

$$Zn(OH)_{ads.} + 2OH^- = Zn(OH)_3^- + e(rds) \quad (2)$$

In near neutral environment, predominant Zn species have been identified to be tetrahedral $Zn(OH)_4^{2-}$.

$$Zn(OH)_3^- + OH^- = Zn(OH)_4^{2-} \quad (3)$$

$$Zn(OH)_4^{2-} = Zn(OH)_2 + 2OH^- \quad (4)$$

$$Zn + 2OH^- = Zn(OH)_2 + 2e \quad (5)$$

$$Zn + 2OH^- = ZnO + H_2O + 2e \quad (6)$$

According to the above-mentioned reactions, solid $Zn(OH)_2$ and ZnO are formed, with no gas evolution during Zn corrosion. Hydrogen release during Zn corrosion is expected to be negligible contrary to the case of Mg. The presence of $Zn(OH)_4^{2-}$ ions in aqueous solutions generally results in a decrease of the hydrogen reduction rate [119]. The stability of both $Zn(OH)_2$ and ZnO is limited by environmental parameters, including presence of hydrogen, carbonates/bicarbonates and phosphates, chloride ions and changes in the concentration of the corrosion products [120]. Furthermore, depending on the mentioned environmental parameters, other Zn compounds can be formed.

Recent studies on Zn and its alloys revealed the presence of several elements such as Zn, P, O, C, Cl, and Ca among the corrosion products after the *in vitro* degradation tests, implying that these products are mainly based on calcium phosphates and carbonates [42,43,64]. The oxygen content may imply the precipitation of oxides and insoluble hydroxides. This is probably a result of the ionic interaction between Zn corrosion products and a series of acidic radicals such as Cl^-, HCO_3^-, HPO_4^{2-} [121]. The stability of Zn compounds has been found to affect the corrosion resistance of zinc in many environments. The dissolution of

zinc may be greatly inhibited by the formation of solid surface films in solutions containing carbonates according to the following reactions [119]:

$$ZnO+2H^{+} \leftrightarrow Zn^{2+} + H_2O \tag{7}$$

$$Zn^{2+} + H_2CO_3 \leftrightarrow ZnCO_{3(s)} + 2H^{+} \tag{8}$$

$$5Zn^{2+} + 2HCO_3^{-} + 6H_2O \leftrightarrow Zn_5(OH)_6(CO_3)_{2(s)} + 8H^{+} \tag{9}$$

$$2H_2 + 2HCO_3^{-} + H_2O + 5ZnO_{(S)} \leftrightarrow Zn_5(OH)_6(CO_3)_{2(s)} \tag{10}$$

The presence of carbonates and bicarbonates extends the possible passivation region to near neutral pH values.

In the presence of Cl^{-}, Zn^{2+} may be able to form various soluble species, such as $ZnCl_2$, $ZnCl_2^{-}$ and surface-confined b-ZnOHCl, that can lead to the formation of the main product of zinc hydroxychloride, $Zn_5(OH)_8Cl_2$. Also for this case, intermediate corrosion products formed on the surface can prevent direct exposure to the environment. In particular, $Zn_5(OH)_8Cl_2 \cdot H_2O$ (simonkolleite) contributes to the improvement of corrosion resistance [122]:

$$\begin{aligned} &5ZnO + 2Cl^{-} + 6H_2O \leftrightarrow Zn_5(OH)_8Cl_2H_2O + 2OH^{-} \cdot 5ZnO + 2Cl^{-} + 6H_2O \\ &\leftrightarrow Zn_5(OH)_8Cl_2 \cdot 2H_2O + 2OH^{-} \end{aligned} \tag{11}$$

In phosphate containing solutions, the dissolution of zinc occurs through a solid surface film whose composition and structure are affected by the pH. At pH < 12 a solid-phase process dominates. It has been reported that the presence of HPO_4^{2-} ions inhibits dissolution of Zn, forming insoluble phosphates such as $ZnHPO_4$ [119]. Passive films formed during Zn dissolution may have different compositions and various degrees of compactness and thus may significantly affect the dissolution process [119].

Addition of alloying elements gives an opportunity to further modulate the corrosion properties of Zn-based bioabsorbable metals in terms of the rate/uniformity of corrosion and mechanical integrity of the implant during the serving period. The corrosion of pure Zn depends more on the properties of Zn itself, while in Zn-based alloys corrosion is mainly related to the size/distribution and fraction of the second phases. The differences in corrosion rates of the investigated Zn-based alloys listed in Table 1 are ascribed to the presence of various second phases such as Mg_2Zn_{11}, $CaZn_{13}$, $SrZn_{13}$, Mg_3Bi_2, $FeZn_{13}$, $AgZn_3$, etc. [43,44,48,74,101]. Even minor changes in the elemental composition of an alloy could significantly alter the degradation mode compared to that of pure Zn. Alloying elements are involved in formulation of new phases in the structure of metal, and each phase has its individual electrochemical properties. Due to the galvanic coupling between second

phases and surrounding matrix, the former are the initiation sites for localized corrosion. Subsequent alloy processing, such as thermal and/or thermomechanical treatments, result in a tailored microstructure with homogenously distributed second phases, promoting more uniform corrosion which is the desirable mode in biomaterials applications.

For instance, Mostaed at al. [43] investigated the influence of grain size on the corrosion performance of pure Zn, Zn-Mg and Zn-Al alloys. A slight reduction in corrosion rates and homogenous corrosion attack due to annealing and extrusion was observed because of the refinement and redistribution of intermetallic particles in extruded Zn-Mg alloys. Additionally, study of mechanical integrity during degradation indicated that in Zn-Mg alloys with an increasing fraction of Mg_2Zn_{11} phase led to a larger rate of loss of material mechanical integrity. In contrast, Zn–Al alloys revealed a slower loss of mechanical integrity as a result of the higher solubility of Al and, thereby, an absence of any second phase particles.

Another studyconducted by the same group indicated that in the case of Zn-Ag alloys, micro-galvanic corrosion is more pronounced in the samples with higher Ag content such as Zn-5.0Ag and Zn-7.0Ag, which is ascribed to the higher volume fraction of $AgZn_3$ second phase particles acting as anodic sites [44]. Similar findings have been reported by Torne et al. [90], who indicated a distinct galvanic coupling in corroded Zn-4.0Ag between $AgZn_3$ dendrites and Zn matrix, leading to an enrichment of $AgZn_3$ phase on the surface of the alloy. However, any Zn-Ag alloy with a solid solution microstructure (no evidence of secondary particles or solute segregation) exhibits a uniform corrosion with no particular pitting corrosion [44]. In brief, understanding the metallurgy of the specific material can help to achieve final microstructures designed to achieve optimal mechanical properties and to provide safe and long-term controlled corrosion.

4. Conclusion and insight for future

An ideal bioabsorbable stent material should possess a corrosion rate matching the tissue healing rate, sufficient mechanical properties and acceptable biocompatibility. Over the last several years, metallurgical attempts have failed to fully achieve all of these objectives in a single material, although Fe and Mg alloys have shown promising properties for bioabsorbable medical devices. Zn has been recently added to the short list of bioabsorbable metal candidates, especially for stent applications, due to its near-ideal corrosion rate and acceptable biocompatibility. Zinc’s low mechanical strength has prompted a search for Zn alloys with enhanced mechanical properties through alloy elemental composition and processing manipulation. To develop novel biomedical Zn alloys both the elemental composition and processing route need to be optimized to achieve desired microstructural characteristics including grain refinement, control over the second phase particles size and distribution, and favorable crystallographic texture orientation, preserving at the same time favorable corrosion rate and biocompatibility.

In this report, the most recent advances in formulation of Zn alloys, their opportunities and limitations have been critically reviewed. In particular, mechanical performance, degradation behavior and *in vivo* investigations have been evaluated for Zn alloys containing various

elements, in either fairly large quantities or traces, developed for medical applications mainly in the last three years.

To date, corrosion studies have been focused mainly on calculation of the material degradation rate. However, a detailed investigation on the corrosion initiation, its progression, formation, growth and biocompatibility of corrosion products and their precise identification still remains unexplored. *In vitro* corrosion mechanism of Zn is mainly dictated by experimental variables such as choice of solution, its electrolyte composition and alkalinity, duration of the test, and samples' surface finish, which vary broadly from experiment to experiment. As a result, a direct comparison between the reported testing results remains a challenge. Additionally, many *in vitro* and *in vivo* studies do not provide accurate specification of materials and samples used such as accurate elemental composition, microstructure characteristics, sample dimensions, ratio of surface area to solution volume, sample surface finish, pH of solution and its stability, etc. Zn materials corrode differently than Mg alloys and development of standardized protocols for this new biomaterial is necessary to simplify the comparison between reported experimental results.

Zinc and its alloys were introduced as biocompatible and biodegradable metals just a few years ago and they still remain under this category after an upsurge of research activities in the biomedical field with this new class of biomaterials. Research with zinc materials has broadened globally in the last three years, but no alarming evidence of cytotoxicity effects associated with biocorossion of zinc materials has been published. As a result, extensive investigations will likely continue in the field of development of bioabsorbable Zn alloys toward getting proper compositions and meeting the strict clinical criteria for vascular scaffolding applications such as excellent biocompatibility, prolonged mechanical integrity and controlled corrosion rate.

Acknowledgments

Jaroslaw Drelich would like to acknowledge U.S. National Institute of Health – National Institute of Biomedical Imaging and Bioengineering (Grant #5R21 EB 019118-02) for the support of his contribution to this paper. He also expresses his appreciation to Adam Drelich for his assistance with editing the manuscript.

References

1. Hermawan H, Dubé D, Mantovani D. Developments in metallic biodegradable stents. Acta Biomater. 62010; :1693–1697. DOI: 10.1016/j.actbio.2009.10.006 [PubMed: 19815097]
2. El-Omar MM, Dangas G, Iakovou I, Mehran R. Update on In-stent Restenosis. Curr. Interv. Cardiol. Rep. 32001; :296–305. [PubMed: 11696295]
3. Schömig A, Kastrati A, Mudra H, Blasini R, Schühlen H, Klauss V, Richardt G, Neumann FJ. Four-year experience with Palmaz-Schatz stenting in coronary angioplasty complicated by dissection with threatened or present vessel closure. Circulation. 901994; :2716–2724. [PubMed: 7994813]
4. Hascoët S, Baruteau A, Jalal Z, Mauri L, Acar P, Elbaz M, Boudjemline Y, Fraisse A. Stents in paediatric and adult congenital interventional cardiac catheterization. Arch. Cardiovasc. Dis. 1072014; :462–475. DOI: 10.1016/j.acvd.2014.06.005 [PubMed: 25128078]
5. Heublein B, Rohde R, Kaese V, Niemeyer M, Hartung W, Haverich A. Biocorrosion of magnesium alloys: a new principle in cardiovascular implant technology? Heart. 892003; :651–656. [PubMed: 12748224]

6. Ong ATL, McFadden EP, Regar E, de Jaegere PPT, van Domburg RT, Serruys PW. Late angiographic stent thrombosis (LAST) events with drug-eluting stents. J. Am. Coll. Cardiol. 452005; :2088–2092. DOI: 10.1016/j.jacc.2005.02.086 [PubMed: 15963413]
7. Bowen PK, Shearier ER, Zhao S, Guillory RJ, Zhao F, Goldman J, Drelich JW. Biodegradable Metals for Cardiovascular Stents: from Clinical Concerns to Recent Zn-Alloys. Adv. Healthc. Mater. 52016; :1121–1140. DOI: 10.1002/adhm.201501019 [PubMed: 27094868]
8. Bowen PK, Drelich J, Goldman J. Zinc Exhibits Ideal Physiological Corrosion Behavior for Bioabsorbable Stents. Adv. Mater. 252013; :2577–2582. DOI: 10.1002/adma.201300226 [PubMed: 23495090]
9. Werkhoven, RJ, Sillekens, WH, van Lieshout, JBJM. Magnes. Technol. Springer: Cham, 2011; 2011. Processing Aspects of Magnesium Alloy Stent Tube; 419–424. https://link.springer.com/chapter/10.1007/978-3-319-48223-1_79 [accessed October 23, 2017]
10. Poncin P, Millet C, Chevy J, Proft JL. Comparing and Optimizing Co-Cr Tubing for Stent Applications. 2004
11. Poncin, P; Proft, J. Stent Tubing: Understanding the Desired Attributes, Materials and Processes for Medical Devices. Presented at Process for Medical Devices Conference; Anaheim, CA. ASM International; Sept 8–10, 2003; n.d.
12. Seitz J-M, Durisin M, Goldman J, Drelich JW. Recent Advances in Biodegradable Metals for Medical Sutures: A Critical Review. Adv. Healthc. Mater. 42015; :1915–1936. DOI: 10.1002/adhm.201500189 [PubMed: 26172399]
13. Bünger CM, Grabow N, Sternberg K, Kröger C, Ketner L, Schmitz K-P, Kreutzer HJ, Ince H, Nienaber CA, Klar E, Schareck W. Sirolimus-Eluting Biodegradable Poly-l-Lactide Stent for Peripheral Vascular Application: A Preliminary Study in Porcine Carotid Arteries. J. Surg. Res. 1392007; :77–82. DOI: 10.1016/j.jss.2006.07.035 [PubMed: 17292417]
14. Im SH, Jung Y, Kim SH. Current status and future direction of biodegradable metallic and polymeric vascular scaffolds for next-generation stents. Acta Biomater. 602017; :3–22. DOI: 10.1016/j.actbio.2017.07.019 [PubMed: 28716610]
15. Ernstberger T, Buchhorn G, Heidrich G. Artifacts in spine magnetic resonance imaging due to different intervertebral test spacers: an in vitro evaluation of magnesium versus titanium and carbon-fiber-reinforced polymers as biomaterials. Neuroradiology. 512009; :525–529. DOI: 10.1007/s00234-009-0537-4 [PubMed: 19468722]
16. Grabow N, Bünger CM, Schultze C, Schmohl K, Martin DP, Williams SF, Sternberg K, Schmitz K-P. A biodegradable slotted tube stent based on poly(L-lactide) and poly(4-hydroxybutyrate) for rapid balloon-expansion. Ann. Biomed. Eng. 352007; :2031–2038. DOI: 10.1007/s10439-007-9376-9 [PubMed: 17846893]
17. Zheng YF, Gu XN, Witte F. Biodegradable metals. Mater. Sci. Eng. R Rep. 772014; :1–34. DOI: 10.1016/j.mser.2014.01.001
18. Qiang G, Mostaed E, Zanella C, Zhentao Y, Vedani M. Ultra-Fine Grained Degradable Magnesium for Biomedical Applications. Rare Met. Mater. Eng. 432014; :2561–2566. DOI: 10.1016/S1875-5372(15)60001-7
19. Mostaed E, Vedani M, Hashempour M, Bestetti M. Influence of ECAP process on mechanical and corrosion properties of pure Mg and ZK60 magnesium alloy for biodegradable stent applications. Biomatter. 42014; :e28283.doi: 10.4161/biom.28283 [PubMed: 25482411]
20. Pierson D, Edick J, Tauscher A, Pokorney E, Bowen P, Gelbaugh J, Stinson J, Getty H, Lee CH, Drelich J, Goldman J. A simplified in vivo approach for evaluating the bioabsorbable behavior of candidate stent materials. J. Biomed. Mater. Res. B Appl. Biomater. 100B2012; :58–67. DOI: 10.1002/jbm.b.31922
21. Zheng, Y. Magnesium Alloys as Degradable Biomaterials. CRC Press; 2015.
22. Saris N-EL, Mervaala E, Karppanen H, Khawaja JA, Lewenstam A. Magnesium: An update on physiological, clinical and analytical aspects. Clin. Chim. Acta. 2942000; :1–26. DOI: 10.1016/S0009-8981(99)00258-2 [PubMed: 10727669]
23. Al-Abdullat Y, Tsutsumi S, Nakajima N, Ohta M, Kuwahara H, Ikeuchi K. Surface modification of magnesium by NaHCO3 and corrosion behavior in Hank's solution for new biomaterial applications. Mater. Trans. 422001; :1777–1780. DOI: 10.2320/matertrans.42.1777

24. Gu X, Zheng Y, Zhong S, Xi T, Wang J, Wang W. Corrosion of, and cellular responses to Mg-Zn-Ca bulk metallic glasses. Biomaterials. 312010; :1093–1103. DOI: 10.1016/j.biomaterials.2009.11.015 [PubMed: 19939446]
25. Li L, Gao J, Wang Y. Evaluation of cyto-toxicity and corrosion behavior of alkali-heat-treated magnesium in simulated body fluid. Surf. Coat. Technol. 1852004; :92–98. DOI: 10.1016/j.surfcoat.2004.01.004
26. Hiromoto S, Yamamoto A. Control of degradation rate of bioabsorbable magnesium by anodization and steam treatment. Mater. Sci. Eng. C. 302010; :1085–1093. DOI: 10.1016/j.msec.2010.06.001
27. [accessed October 23, 2017] EuroPCR 2016: Magmaris*, the first clinically proven bioresorbable magnesium scaffold, shows long-term safety in BIOSOLVE-II Trial. (n.d.) https://www.pcronline.com/News/Press-releases/2016/EuroPCR-2016-Magmaris-the-first-clinically-proven-bioresorbable-magnesium-scaffold-shows-long-term-safety-in-BIOSOLVE-II-Trial
28. Trumbo P, Schlicker S, Yates AA, Poos M. Dietary reference intakes for energy, carbohydrate, fiber, fat, fatty acids, cholesterol, protein and amino acids. J. Am. Diet. Assoc. 1022002; :1621–1630. DOI: 10.1016/S0002-8223(02)90346-9 [PubMed: 12449285]
29. Peuster M, Wohlsein P, Brügmann M, Ehlerding M, Seidler K, Fink C, Brauer H, Fischer A, Hausdorf G. A novel approach to temporary stenting: degradable cardiovascular stents produced from corrodible metal—results 6–18 months after implantation into New Zealand white rabbits. Heart. 862001; :563–569. DOI: 10.1136/heart.86.5.563 [PubMed: 11602554]
30. Ohlmann P, Mintz GS, Kim S-W, Pichard AD, Satler LF, Kent KM, Suddath WO, Waksman R, Weissman NJ. Intravascular ultrasound findings in patients with restenosis of sirolimus- and paclitaxel-eluting stents. Int. J. Cardiol. 1252008; :11–15. DOI: 10.1016/j.ijcard.2007.02.021 [PubMed: 17442432]
31. Peuster M, Hesse C, Schloo T, Fink C, Beerbaum P, von S. Long-term biocompatibility of a corrodible peripheral iron stent in the porcine descending aorta. Biomaterials. 272006; :4955–4962. DOI: 10.1016/j.biomaterials.2006.05.029 [PubMed: 16765434]
32. Sikora-Jasinska M, Paternoster C, Mostaed E, Tolouei R, Casati R, Vedani M, Mantovani D. Synthesis, mechanical properties and corrosion behavior of powder metallurgy processed Fe/Mg2Si composites for biodegradable implant applications. Mater. Sci. Eng. C. 812017; :511–521. DOI: 10.1016/j.msec.2017.07.049
33. Moravej M, Purnama A, Fiset M, Couet J, Mantovani D. Electroformed pure iron as a new biomaterial for degradable stents: In vitro degradation and preliminary cell viability studies. Acta Biomater. 62010; :1843–1851. DOI: 10.1016/j.actbio.2010.01.008 [PubMed: 20080213]
34. Tapiero H, Tew KD. Trace elements in human physiology and pathology: zinc and metallothioneins. Biomed. Pharmacother. 572003; :399–411. DOI: 10.1016/S0753-3322(03)00081-7 [PubMed: 14652165]
35. Hambidge M. Human Zinc Deficiency. J. Nutr. 1302000; :1344S–1349S. [PubMed: 10801941]
36. Rink L. Zinc and the immune system. Proc. Nutr. Soc. 592000; :541–552. DOI: 10.1017/S0029665100000781 [PubMed: 11115789]
37. Zhang S, Zhang X, Zhao C, Li J, Song Y, Xie C, Tao H, Zhang Y, He Y, Jiang Y, Bian Y. Research on an Mg–Zn alloy as a degradable biomaterial. Acta Biomater. 62010; :626–640. DOI: 10.1016/j.actbio.2009.06.028 [PubMed: 19545650]
38. Apelian D, Paliwal M, Herrschaft DC. Casting with Zinc Alloys. JOM. 331981; :12–20. DOI: 10.1007/BF03339527
39. Drelich AJ, Zhao S, Guillory RJ, Drelich JW, Goldman J. Long-term surveillance of zinc implant in murine artery: Surprisingly steady biocorrosion rate. Acta Biomater. 582017; :539–549. DOI: 10.1016/j.actbio.2017.05.045 [PubMed: 28532901]
40. Drelich AJ, Bowen PK, LaLonde L, Goldman J, Drelich JW. Importance of oxide film in endovascular biodegradable zinc stents. Surf. Innov. 42016; :133–140. DOI: 10.1680/jsuin.16.00014
41. Shomali AA, Guillory RJ, Seguin D, Goldman J, Drelich JW. Effect of PLLA coating on corrosion and biocompatibility of zinc in vascular environment. Surf. Innov. 52017; :211–220. DOI: 10.1680/jsuin.17.00011

42. Vojtěch D, Kubásek J, Šerák J, Novák P. Mechanical and corrosion properties of newly developed biodegradable Zn-based alloys for bone fixation. Acta Biomater. 72011; :3515–3522. DOI: 10.1016/j.actbio.2011.05.008 [PubMed: 21621017]
43. Mostaed E, Sikora-Jasinska M, Mostaed A, Loffredo S, Demir AG, Previtali B, Mantovani D, Beanland R, Vedani M. Novel Zn-based alloys for biodegradable stent applications: Design, development and in vitro degradation. J. Mech. Behav. Biomed. Mater. 602016; :581–602. DOI: 10.1016/j.jmbbm.2016.03.018 [PubMed: 27062241]
44. Sikora-Jasinska M, Mostaed E, Mostaed A, Beanland R, Mantovani D, Vedani M. Fabrication, mechanical properties and in vitro degradation behavior of newly developed ZnAg alloys for degradable implant applications. Mater. Sci. Eng. C. 772017; :1170–1181. DOI: 10.1016/j.msec.2017.04.023
45. Shen C, Liu X, Fan B, Lan P, Zhou F, Li X, Wang H, Xiao X, Li L, Zhao S, Guo Z, Pu Z, Zheng Y. Mechanical properties, in vitro degradation behavior, hemocompatibility and cytotoxicity evaluation of Zn–1.2Mg alloy for biodegradable implants. RSC Adv. 62016; :86410–86419. DOI: 10.1039/C6RA14300H
46. Yokel RA, McNamara PJ. Aluminium Toxicokinetics: An Updated MiniReview. Pharmacol. Toxicol. 882001; :159–167. DOI: 10.1111/j.1600-0773.2001.880401.x [PubMed: 11322172]
47. Zhao S, Seitz J-M, Eifler R, Maier HJ, Guillory RJ II, Earley EJ, Drelich A, Goldman J, Drelich JW. Zn-Li alloy after extrusion and drawing: Structural, mechanical characterization, and biodegradation in abdominal aorta of rat. Mater. Sci. Eng. C. 762017; :301–312. DOI: 10.1016/j.msec.2017.02.167
48. Li HF, Xie XH, Zheng YF, Cong Y, Zhou FY, Qiu KJ, Wang X, Chen SH, Huang L, Tian L, Qin L. Development of biodegradable Zn-1X binary alloys with nutrient alloying elements Mg, Ca and Sr. Sci. Rep. 52015; :10719.doi: 10.1038/srep10719 [PubMed: 26023878]
49. Bowen PK, Seitz J-M, Guillory RJ, Braykovich JP, Zhao S, Goldman J, Drelich JW. Evaluation of wrought Zn–Al alloys (1, 3, and 5 wt % Al) through mechanical and in vivo testing for stent applications. J. Biomed. Mater. Res. B Appl. Biomater. 2017; :n/a–n/a. DOI: 10.1002/jbm.b.33850
50. Niu J, Tang Z, Huang H, Pei J, Zhang H, Yuan G, Ding W. Research on a Zn-Cu alloy as a biodegradable material for potential vascular stents application. Mater. Sci. Eng. C. 692016; :407–413. DOI: 10.1016/j.msec.2016.06.082
51. Liu X, Sun J, Zhou F, Yang Y, Chang R, Qiu K, Pu Z, Li L, Zheng Y. Micro-alloying with Mn in Zn–Mg alloy for future biodegradable metals application. Mater. Des. 942016; :95–104. DOI: 10.1016/j.matdes.2015.12.128
52. Bakhsheshi-Rad HR, Hamzah E, Low HT, Kasiri-Asgarani M, Farahany S, Akbari E, Cho MH. Fabrication of biodegradable Zn-Al-Mg alloy: Mechanical properties, corrosion behavior, cytotoxicity and antibacterial activities. Mater. Sci. Eng. C. 732017; :215–219. DOI: 10.1016/j.msec.2016.11.138
53. Liu X, Sun J, Yang Y, Pu Z, Zheng Y. In vitro investigation of ultra-pure Zn and its mini-tube as potential bioabsorbable stent material. Mater. Lett. 1612015; :53–56. DOI: 10.1016/j.matlet.2015.06.107
54. Liu X, Sun J, Qiu K, Yang Y, Pu Z, Li L, Zheng Y. Effects of alloying elements (Ca and Sr) on microstructure, mechanical property and in vitro corrosion behavior of biodegradable Zn–1.5Mg alloy. J. Alloys Compd. Complete. 2016; :444–452. DOI: 10.1016/j.jallcom.2015.10.116
55. Li H, Yang H, Zheng Y, Zhou F, Qiu K, Wang X. Design and characterizations of novel biodegradable ternary Zn-based alloys with IIA nutrient alloying elements Mg, Ca and Sr. Mater. Des. 832015; :95–102. DOI: 10.1016/j.matdes.2015.05.089
56. Ding Y, Wen C, Hodgson P, Li Y. Effects of alloying elements on the corrosion behavior and biocompatibility of biodegradable magnesium alloys: a review. J. Mater. Chem. B. 22014; :1912–1933. DOI: 10.1039/C3TB21746A
57. Zhang L-N, Hou Z-T, Ye X, Xu Z-B, Bai X-L, Shang P. The effect of selected alloying element additions on properties of Mg-based alloy as bioimplants: A literature review. Front. Mater. Sci. 72013; :227–236. DOI: 10.1007/s11706-013-0210-z

58. Liu X, Sun J, Yang Y, Zhou F, Pu Z, Li L, Zheng Y. Microstructure, mechanical properties, in vitro degradation behavior and hemocompatibility of novel Zn–Mg–Sr alloys as biodegradable metals. Mater. Lett. 1622016; :242–245. DOI: 10.1016/j.matlet.2015.07.151
59. Jin H, Zhao S, Guillory R, Bowen PK, Yin Z, Griebel A, Schaffer J, Earley EJ, Goldman J, Drelich JW. Novel high-strength, low-alloys Zn-Mg (<0.1wt% Mg) and their arterial biodegradation. Mater. Sci. Eng. C. 842018; :67–79. DOI: 10.1016/j.msec.2017.11.021
60. Wang L, He Y, Zhao H, Xie H, Li S, Ren Y, Qin G. Effect of cumulative strain on the microstructural and mechanical properties of Zn-0.02wt.%Mg alloy wires during room-temperature drawing process. J. Alloys Compd.
61. William, D, Callister, D. Materials Science and Engineering: An Introduction. John Wile, John Wiley and Sons; Hoboken NJ: 2009. 2009
62. Gong H, Wang K, Strich R, Zhou JG. In vitro biodegradation behavior, mechanical properties, and cytotoxicity of biodegradable Zn–Mg alloy. J. Biomed. Mater. Res. B Appl. Biomater. 2015; :n/a–n/a. DOI: 10.1002/jbm.b.33341
63. Yao C, Wang Z, Tay SL, Zhu T, Gao W. Effects of Mg on microstructure and corrosion properties of Zn–Mg alloy. J. Alloys Compd. 6022014; :101–107. DOI: 10.1016/j.jallcom.2014.03.025
64. Jablonská E, Vojtěch D, Fousová M, Kubásek J, Lipov J, Fojt J, Ruml T. Influence of surface pre-treatment on the cytocompatibility of a novel biodegradable ZnMg alloy. Mater. Sci. Eng. C. 682016; :198–204. DOI: 10.1016/j.msec.2016.05.114
65. Wang C, Yu Z, Cui Y, Zhang Y, Yu S, Qu G, Gong H. Processing of a Novel Zn Alloy Micro-Tube for Biodegradable Vascular Stent Application. J. Mater. Sci. Technol. 322016; :925–929. DOI: 10.1016/j.jmst.2016.08.008
66. Ilich JZ, Kerstetter JE. Nutrition in bone health revisited: a story beyond calcium. J. Am. Coll. Nutr. 192000; :715–737. [PubMed: 11194525]
67. Zhang W, Shen Y, Pan H, Lin K, Liu X, Darvell BW, Lu WW, Chang J, Deng L, Wang D, Huang W. Effects of strontium in modified biomaterials. Acta Biomater. 72011; :800–808. DOI: 10.1016/j.actbio.2010.08.031 [PubMed: 20826233]
68. Dahl SG, Allain P, Marie PJ, Mauras Y, Boivin G, Ammann P, Tsouderos Y, Delmas PD, Christiansen C. Incorporation and distribution of strontium in bone. Bone. 282001; :446–453. DOI: 10.1016/S8756-3282(01)00419-7 [PubMed: 11336927]
69. Li Z, Gu X, Lou S, Zheng Y. The development of binary Mg–Ca alloys for use as biodegradable materials within bone. Biomaterials. 292008; :1329–1344. DOI: 10.1016/j.biomaterials.2007.12.021 [PubMed: 18191191]
70. Greger JL. Dietary and other sources of aluminium intake. Ciba Found. Symp. 1691992; :26–35. 49. [PubMed: 1490425]
71. Kawahara M, Kato-Negishi M. Link between Aluminum and the Pathogenesis of Alzheimer's Disease: The Integration of the Aluminum and Amyloid Cascade Hypotheses. Int. J. Alzheimers Dis. 2011; doi: 10.4061/2011/276393
72. I.L.Z.R. Organization. Engineering properties of zinc alloys. International Lead Zinc Research Organization; 1980.
73. da Costa EM, da Costa CE, Vecchia FD, Rick C, Scherer M, dos Santos CA, Dedavid BA. Study of the influence of copper and magnesium additions on the microstructure formation of Zn–Al hypoeutectic alloys. J. Alloys Compd. 4882009; :89–99. DOI: 10.1016/j.jallcom.2009.08.125
74. Bakhsheshi-Rad HR, Hamzah E, Low HT, Cho MH, Kasiri-Asgarani M, Farahany S, Mostafa A, Medraj M. Thermal Characteristics, Mechanical Properties, In Vitro Degradation and Cytotoxicity of Novel Biodegradable Zn–Al–Mg and Zn–Al–Mg–xBi Alloys. Acta Metall. Sin. Engl. Lett. 302017; :201–211. DOI: 10.1007/s40195-017-0534-2
75. Wang C, Yang HT, Li X, Zheng YF. In Vitro Evaluation of the Feasibility of Commercial Zn Alloys as Biodegradable Metals. J. Mater. Sci. Technol. 322016; :909–918. DOI: 10.1016/j.jmst.2016.06.003
76. Ferner RE, Smith JM, Koren G. Lithium and pregnancy. The Lancet. 3391992; :869.doi: 10.1016/0140-6736(92)90311-P

77. Aral H, Vecchio-Sadus A. Toxicity of lithium to humans and the environment-A literature review. Ecotoxicol. Environ. Saf. 702008; :349–356. DOI: 10.1016/j.ecoenv.2008.02.026 [PubMed: 18456327]

78. Young W. Review of Lithium Effects on Brain and Blood. Cell Transplant. 182009; :951–975. DOI: 10.3727/096368909X471251 [PubMed: 19523343]

79. Zeng R-C, Sun L, Zheng Y-F, Cui H-Z, Han E-H. Corrosion and characterisation of dual phase Mg–Li–Ca alloy in Hank's solution: The influence of microstructural features. Corros. Sci. 792014; :69–82. DOI: 10.1016/j.corsci.2013.10.028

80. Liu Y, Wu Y, Bian D, Gao S, Leeflang S, Guo H, Zheng Y, Zhou J. Study on the Mg-Li-Zn ternary alloy system with improved mechanical properties, good degradation performance and different responses to cells. Acta Biomater. 622017; :418–433. DOI: 10.1016/j.actbio.2017.08.021 [PubMed: 28823717]

81. Zhao S, McNamara CT, Bowen PK, Verhun N, Braykovich JP, Goldman J, Drelich JW. Structural Characteristics and In Vitro Biodegradation of a Novel Zn-Li Alloy Prepared by Induction Melting and Hot Rolling. Metall. Mater. Trans. A. 482017; :1204–1215. DOI: 10.1007/s11661-016-3901-0

82. D T, F F, Wd M, R S, K L, Ku K, R W. Antibacterial biodegradable Mg-Ag alloys. Eur. Cell. Mater. 252013; :284–98. [PubMed: 23771512]

83. Hadrup N, Lam HR. Oral toxicity of silver ions, silver nanoparticles and colloidal silver – A review. Regul. Toxicol. Pharmacol. 682014; :1–7. DOI: 10.1016/j.yrtph.2013.11.002 [PubMed: 24231525]

84. Chernousova S, Epple M. Silver as Antibacterial Agent: Ion, Nanoparticle, and Metal. Angew. Chem. Int. Ed. 522013; :1636–1653. DOI: 10.1002/anie.201205923

85. VanOosten SK, Yuca E, Karaca BT, Boone K, Snead ML, Spencer P, Tamerler C. Biosilver nanoparticle interface offers improved cell viability. Surf. Innov. 42016; :121–132. DOI: 10.1680/jsuin.16.00010 [PubMed: 29057075]

86. Zhang BB, Zheng YF, Liu Y. Effect of Ag on the corrosion behavior of Ti–Ag alloys in artificial saliva solutions. Dent. Mater. 252009; :672–677. DOI: 10.1016/j.dental.2008.10.016 [PubMed: 19150734]

87. Fordham WR, Redmond S, Westerland A, Cortes EG, Walker C, Gallagher C, Medina CJ, Waecther F, Lunk C, Ostrum RF, Caputo GA, Hettinger JD, Krchnavek RR. Silver as a Bactericidal Coating for Biomedical Implants. Surf. Coat. Technol. 2532014; :52–57. DOI: 10.1016/j.surfcoat.2014.05.013

88. Simchi A, Tamjid E, Pishbin F, Boccaccini AR. Recent progress in inorganic and composite coatings with bactericidal capability for orthopaedic applications. Nanomedicine Nanotechnol. Biol. Med. 72011; :22–39. DOI: 10.1016/j.nano.2010.10.005

89. Darouiche RO. Treatment of Infections Associated with Surgical Implants. N. Engl. J. Med. 3502004; :1422–1429. DOI: 10.1056/NEJMra035415 [PubMed: 15070792]

90. Törne KB, Khan FA, Örnberg A, Weissenrieder J. Zn–Mg and Zn—Ag degradation mechanism under biologically relevant conditions. Surf. Innov. 2017; :1–12. DOI: 10.1680/jsuin.17.00053

91. Bost M, Houdart S, Oberli M, Kalonji E, Huneau J-F, Margaritis I. Dietary copper and human health: Current evidence and unresolved issues. J. Trace Elem. Med. Biol. 352016; :107–115. DOI: 10.1016/j.jtemb.2016.02.006 [PubMed: 27049134]

92. Harris ED. A Requirement for Copper in Angiogenesis. Nutr. Rev. 622004; :60–64. DOI: 10.1301/nr.2004.feb.60-64 [PubMed: 15080367]

93. Finney L, Vogt S, Fukai T, Glesne D. Copper and angiogenesis: Unravelling a relationship key to cancer progression. Clin. Exp. Pharmacol. Physiol. 362009; :88–94. DOI: 10.1111/j.1440-1681.2008.04969.x [PubMed: 18505439]

94. Uriu-Adams JY, Keen CL. Copper, oxidative stress, and human health. Mol. Aspects Med. 262005; :268–298. DOI: 10.1016/j.mam.2005.07.015 [PubMed: 16112185]

95. Saari JT. Copper deficiency and cardiovascular disease: role of peroxidation, glycation, and nitration. Can. J. Physiol. Pharmacol. 782000; :848–855. DOI: 10.1139/y00-054 [PubMed: 11077985]

96. Chen Q, Thouas GA. Metallic implant biomaterials. Mater. Sci. Eng. R Rep. 872015; :1–57. DOI: 10.1016/j.mser.2014.10.001

97. Borkow G, Gabbay J, Zatcoff RC. Could chronic wounds not heal due to too low local copper levels? Med. Hypotheses. 702008; :610–613. DOI: 10.1016/j.mehy.2007.06.006 [PubMed: 17689198]

98. Drelich AJ, Miller J, Donofrio R, Drelich JW. Novel Durable Antimicrobial Ceramic with Embedded Copper Sub-Microparticles for a Steady-State Release of Copper Ions. Materials. 102017; :775.doi: 10.3390/ma10070775

99. Ren L, Nan L, Yang K. Study of copper precipitation behavior in a Cu-bearing austenitic antibacterial stainless steel. Mater. Des. 322011; :2374–2379. DOI: 10.1016/j.matdes.2010.11.030

100. Tang Z, Huang H, Niu J, Zhang L, Zhang H, Pei J, Tan J, Yuan G. Design and characterizations of novel biodegradable Zn-Cu-Mg alloys for potential biodegradable implants. Mater. Des. 1172017; :84–94. DOI: 10.1016/j.matdes.2016.12.075

101. Yue R, Huang H, Ke G, Zhang H, Pei J, Xue G, Yuan G. Microstructure, mechanical properties and in vitro degradation behavior of novel Zn-Cu-Fe alloys. Mater. Charact. 1342017; :114–122. DOI: 10.1016/j.matchar.2017.10.015

102. Erikson KM, Syversen T, Aschner JL, Aschner M. Interactions between excessive manganese exposures and dietary iron-deficiency in neurodegeneration. Environ. Toxicol. Pharmacol. 192005; :415–421. DOI: 10.1016/j.etap.2004.12.053 [PubMed: 21783506]

103. Sun S, Ren Y, Wang L, Yang B, Li H, Qin G. Abnormal effect of Mn addition on the mechanical properties of as-extruded Zn alloys. Mater. Sci. Eng. A. 7012017; :129–133. DOI: 10.1016/j.msea.2017.06.037

104. Wang J, Witte F, Xi T, Zheng Y, Yang K, Yang Y, Zhao D, Meng J, Li Y, Li W, Chan K, Qin L. Recommendation for modifying current cytotoxicity testing standards for biodegradable magnesium-based materials. Acta Biomater. 212015; :237–249. DOI: 10.1016/j.actbio.2015.04.011 [PubMed: 25890098]

105. Fischer J, Pröfrock D, Hort N, Willumeit R, Feyerabend F. Improved cytotoxicity testing of magnesium materials. Mater. Sci. Eng. B. 1762011; :830–834. DOI: 10.1016/j.mseb.2011.04.008

106. Tang Z, Niu J, Huang H, Zhang H, Pei J, Ou J, Yuan G. Potential biodegradable Zn-Cu binary alloys developed for cardiovascular implant applications. J. Mech. Behav. Biomed. Mater. 722017; :182–191. DOI: 10.1016/j.jmbbm.2017.05.013 [PubMed: 28499166]

107. Shearier ER, Bowen PK, He W, Drelich A, Drelich J, Goldman J, Zhao F. In Vitro Cytotoxicity, Adhesion, and Proliferation of Human Vascular Cells Exposed to Zinc. ACS Biomater. Sci. Eng. 22016; :634–642. DOI: 10.1021/acsbiomaterials.6b00035 [PubMed: 27840847]

108. Ma J, Zhao N, Zhu D. Endothelial Cellular Responses to Biodegradable Metal Zinc. ACS Biomater. Sci. Eng. 12015; :1174–1182. DOI: 10.1021/acsbiomaterials.5b00319 [PubMed: 27689136]

109. Zhu D, Su Y, Young ML, Ma J, Zheng Y, Tang L. Biological Responses and Mechanisms of Human Bone Marrow Mesenchymal Stem Cells to Zn and Mg Biomaterials. ACS Appl. Mater. Interfaces. 92017; :27453–27461. DOI: 10.1021/acsami.7b06654 [PubMed: 28787130]

110. Murni NS, Dambatta MS, Yeap SK, Froemming GRA, Hermawan H. Cytotoxicity evaluation of biodegradable Zn-3Mg alloy toward normal human osteoblast cells. Mater. Sci. Eng. C Mater. Biol. Appl. 492015; :560–566. DOI: 10.1016/j.msec.2015.01.056 [PubMed: 25686984]

111. Guillory RJ, Bowen PK, Hopkins SP, Shearier ER, Earley EJ, Gillette AA, Aghion E, Bocks M, Drelich JW, Goldman J. Corrosion Characteristics Dictate the Long-Term Inflammatory Profile of Degradable Zinc Arterial Implants. ACS Biomater. Sci. Eng. 22016; :2355–2364. DOI: 10.1021/acsbiomaterials.6b00591

112. Bowen PK, Guillory RJ II, Shearier ER, Seitz J-M, Drelich J, Bocks M, Zhao F, Goldman J. Metallic zinc exhibits optimal biocompatibility for bioabsorbable endovascular stents. Mater. Sci. Eng. C. 562015; :467–472. DOI: 10.1016/j.msec.2015.07.022

113. Yang H, Wang C, Liu C, Chen H, Wu Y, Han J, Jia Z, Lin W, Zhang D, Li W, Yuan W, Guo H, Li H, Yang G, Kong D, Zhu D, Takashima K, Ruan L, Nie J, Li X, Zheng Y. Evolution of the degradation mechanism of pure zinc stent in the one-year study of rabbit abdominal aorta model. Biomaterials. 1452017; :92–105. DOI: 10.1016/j.biomaterials.2017.08.022 [PubMed: 28858721]

114. Kubásek J, Vojtěch D, Jablonská E, PospíŠilová I, Lipov J, Ruml T. Structure, mechanical characteristics and in vitro degradation, cytotoxicity, genotoxicity and mutagenicity of novel

biodegradable Zn–Mg alloys. Mater. Sci. Eng. C. 582016; :24–35. DOI: 10.1016/j.msec.2015.08.015

115. Kleiner S, Uggowitzer PJ. Mechanical anisotropy of extruded Mg-6% Al-1% Zn alloy. Mater. Sci. Eng. A. 3792004; :258–263. DOI: 10.1016/j.msea.2004.02.020
116. Mostaed E, Fabrizi A, Dellasega D, Bonollo F, Vedani M. Grain size and texture dependence on mechanical properties, asymmetric behavior and low temperature superplasticity of ZK60 Mg alloy. Mater. Charact. 1072015; :70–78. DOI: 10.1016/j.matchar.2015.06.009
117. Mostaed E, Fabrizi A, Dellasega D, Bonollo F, Vedani M. Microstructure, mechanical behavior and low temperature superplasticity of ECAP processed ZM21 Mg alloy. J. Alloys Compd. 6382015; :267–276. DOI: 10.1016/j.jallcom.2015.03.029
118. Törne K, Larsson M, Norlin A, Weissenrieder J. Degradation of zinc in saline solutions, plasma, and whole blood. J. Biomed. Mater. Res. B Appl. Biomater. 1042016; :1141–1151. DOI: 10.1002/jbm.b.33458 [PubMed: 26061136]
119. Zhang, XG. Corrosion and Electrochemistry of Zinc. Springer Science & Business Media; 2013.
120. Muster TH, Cole IS. The protective nature of passivation films on zinc: surface charge. Corros. Sci. 462004; :2319–2335. DOI: 10.1016/j.corsci.2004.01.002
121. Lévesque J, Hermawan H, Dubé D, Mantovani D. Design of a pseudo-physiological test bench specific to the development of biodegradable metallic biomaterials. Acta Biomater. 42008; :284–295. [PubMed: 18033745]
122. Falk T, Svensson J-E, Johansson L-G. The Influence of CO 2 and NaCl on the Atmospheric Corrosion of Zinc A Laboratory Study. J. Electrochem. Soc. 1451998; :2993–2999. DOI: 10.1149/1.1838753
123. Butts, DA, Gale, WF. 11 - Equilibrium diagrams. In: Totemeier, WFGC, editor. Smithells Met. Ref. Book. Eighth. Butterworth-Heinemann; Oxford: 2004. 1–534. http://www.sciencedirect.com/science/article/pii/B9780750675093500142 [accessed December 20, 2015]
124. Pelton AD. The Li-Zn (Lithium-Zinc) System. J. Phase Equilibria. 121991; :42–45. DOI: 10.1007/BF02663672
125. Wang L-Q, Ren Y-P, Sun S-N, Zhao H, Li S, Qin G-W. Microstructure, Mechanical Properties and Fracture Behavior of As-Extruded Zn–Mg Binary Alloys. Acta Metall. Sin. Engl. Lett. 302017; :931–940. DOI: 10.1007/s40195-017-0585-4

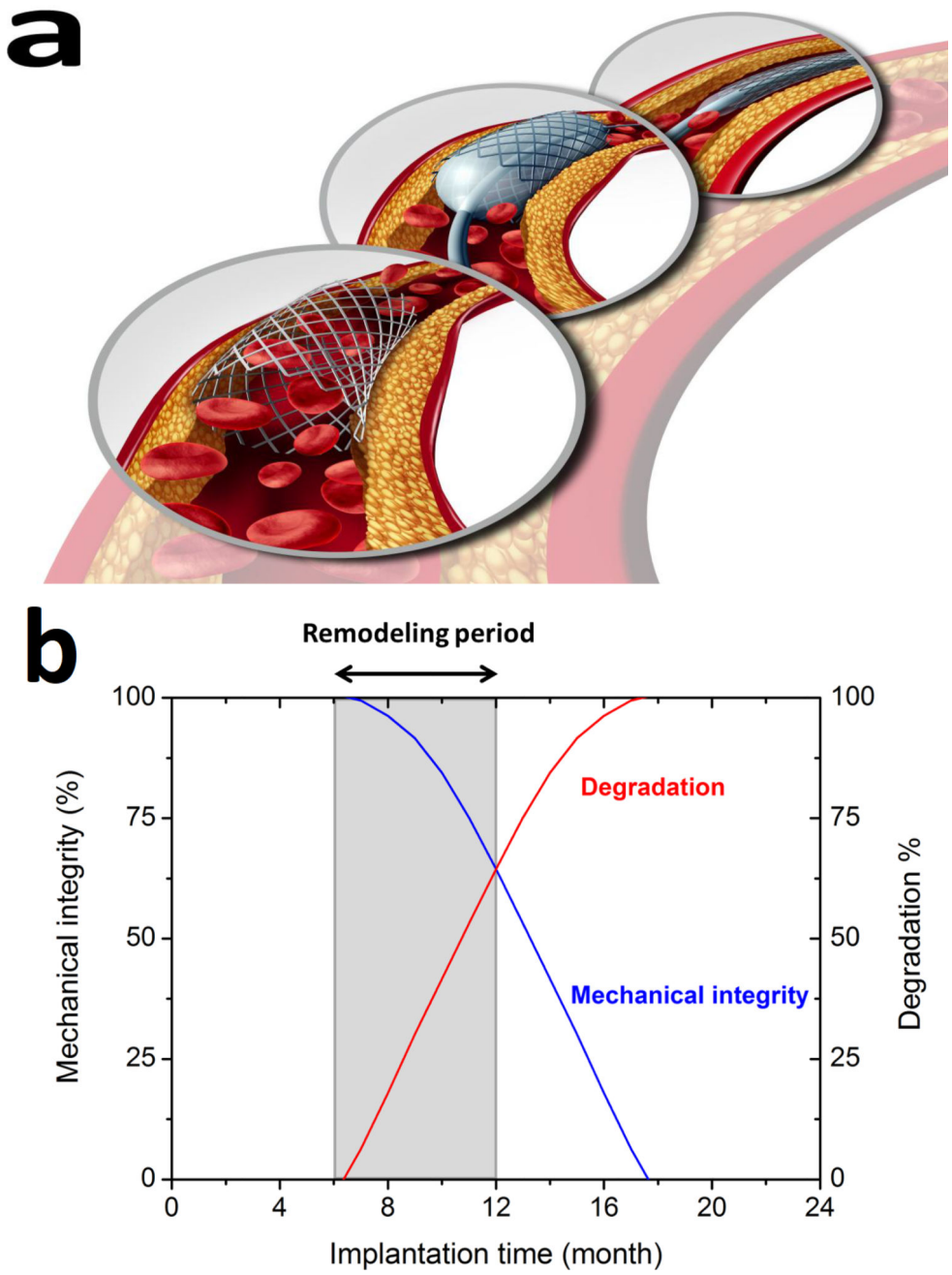

Fig. 1.

(a) Schematic illustration of stent implantation into a coronary vessel, and (b) a compromise between degradation and mechanical integrity of an ideal absorbable stent (prepared based on Ref. [1]).

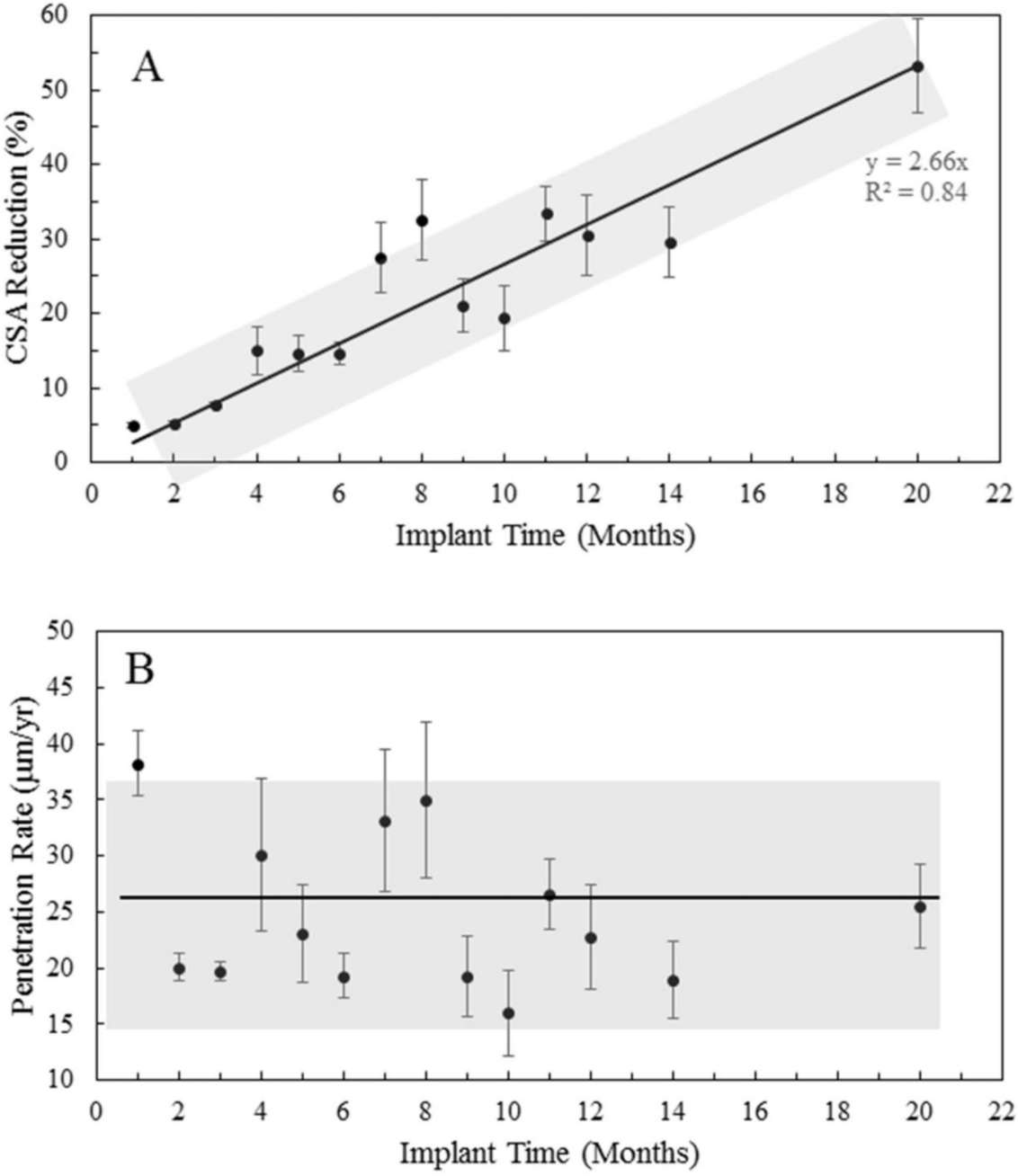

Fig. 2.

Cross-sectional area (CSA) reduction (A) and penetration rate (B) of ϕ0.25 mm zinc wires implanted in abdominal aorta of rats as a function of implantation time. Reproduced from Ref. [39] with permission.

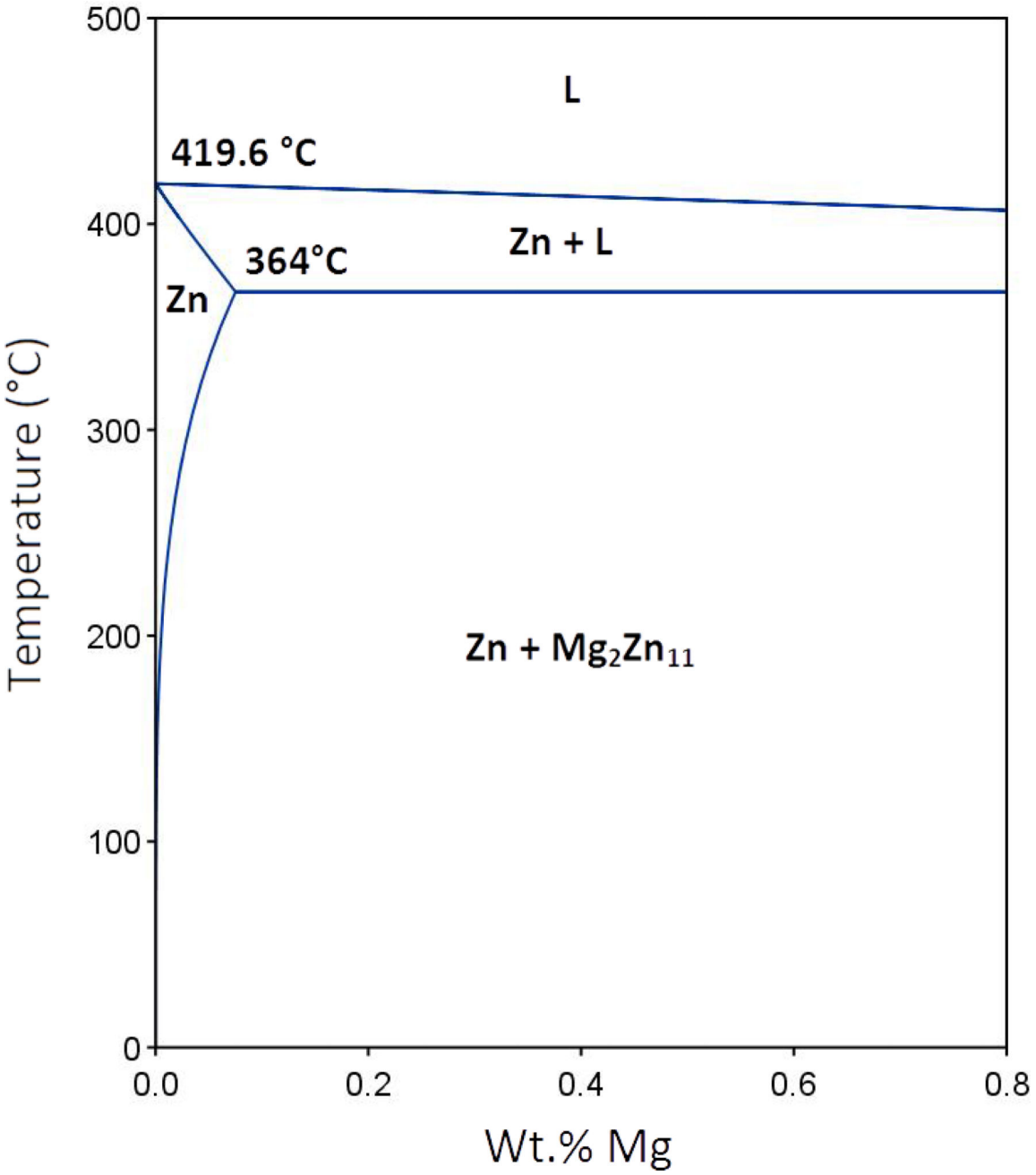

Fig. 3.
Zn-Mg equilibrium phase diagram (based on Ref. [123]).

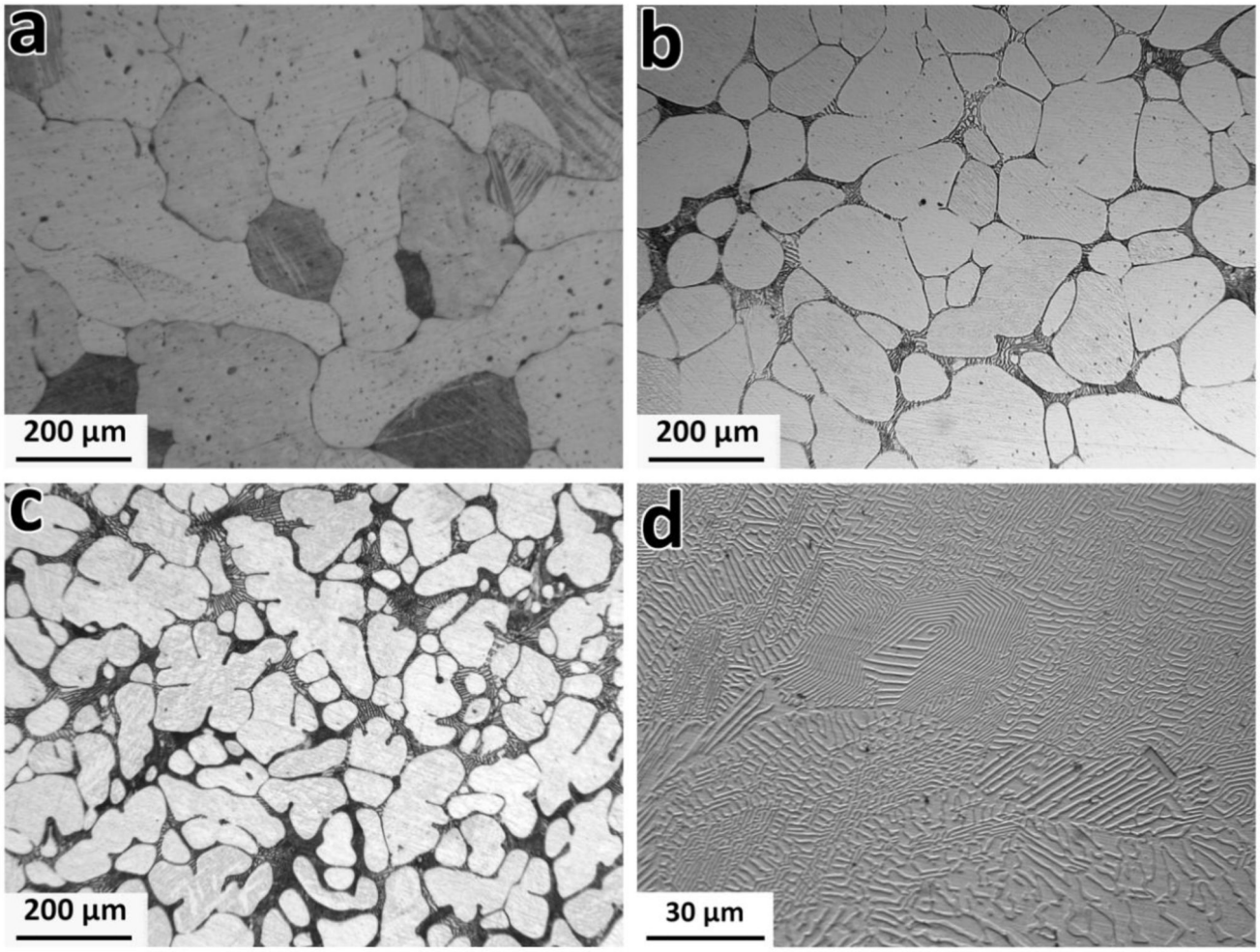

Fig. 4.
Microstructure of the as-cast (a) Zn-0.15Mg, (b) Zn-0.5Mg, (c) Zn-1.0Mg and (d) Zn-3.0Mg alloys.

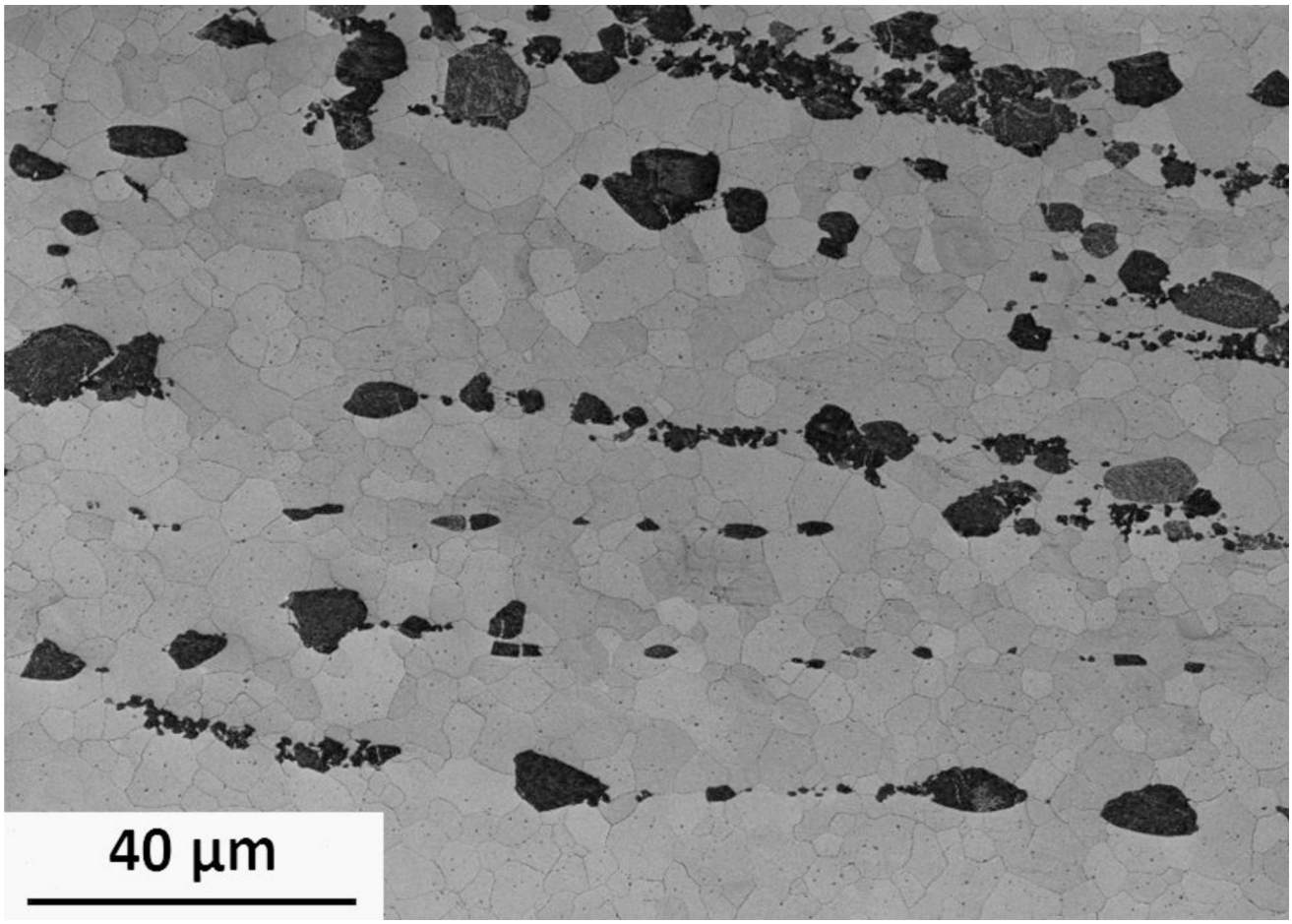

Fig. 5.
Microstructure of the Zn-0.5Mg alloy after hot extrusion at 250°C. Reprinted with permission [43].

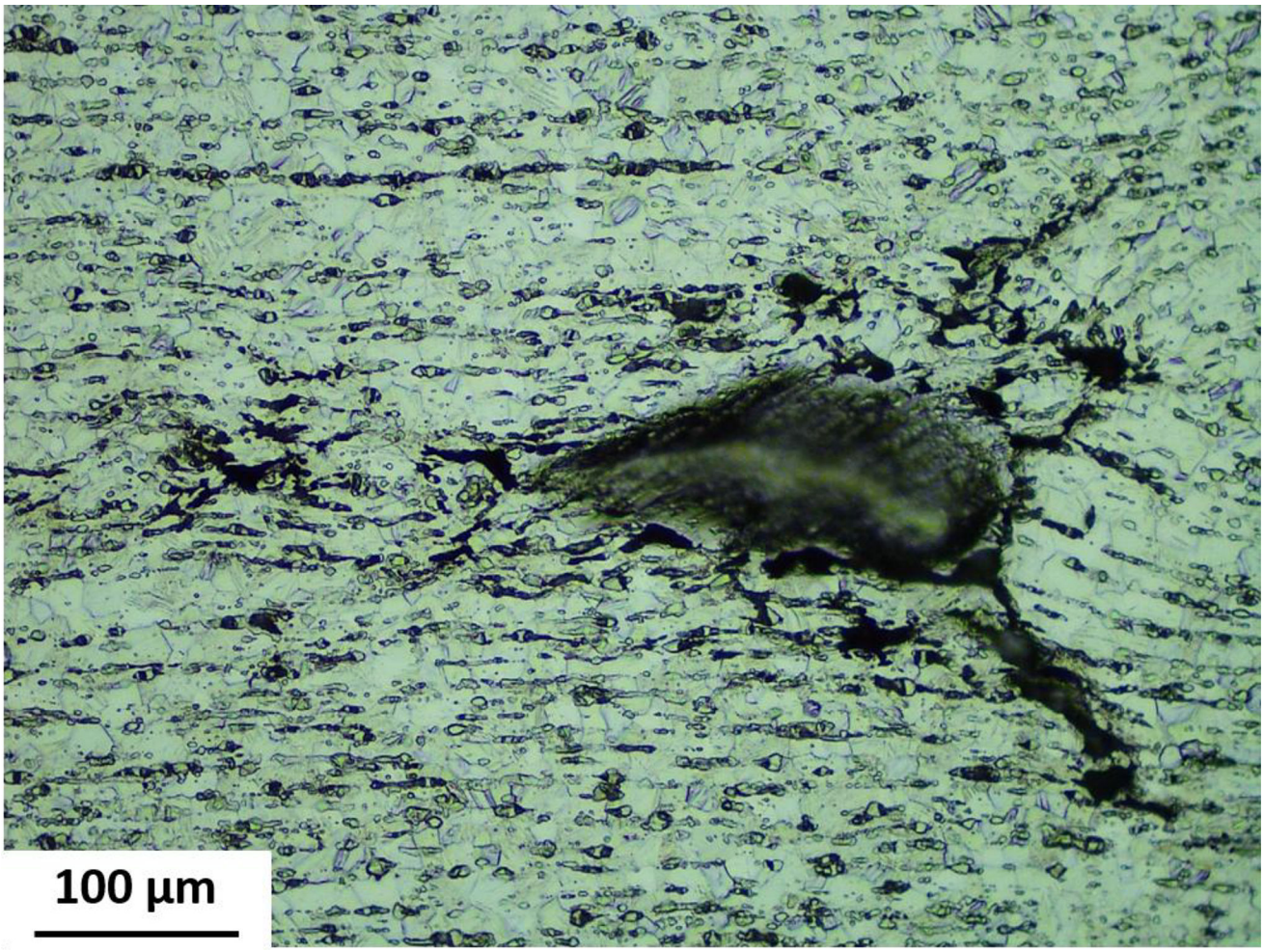

Fig. 6.

Microstructure of a cold drawn Zn-0.5Mg alloy wire to a cumulative strain of 60%, representing the occurrence of internal cracking during cold work processing.

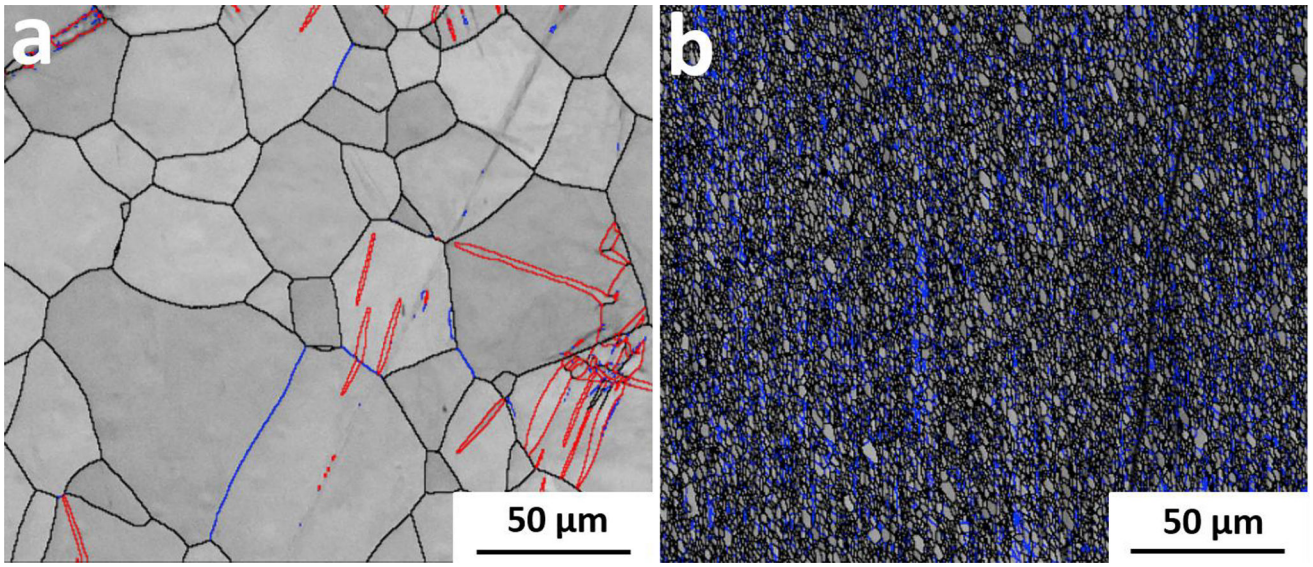

Fig. 7.

Grain boundary misorientation maps of (a) as-extruded and (b) 97% cold drawn Zn-0.02Mg alloy. Blue, black and red lines correspond to LAGB (2°–15°), HAGB (>15°) and extension twin boundaries, respectively. Reprinted with permission [60].

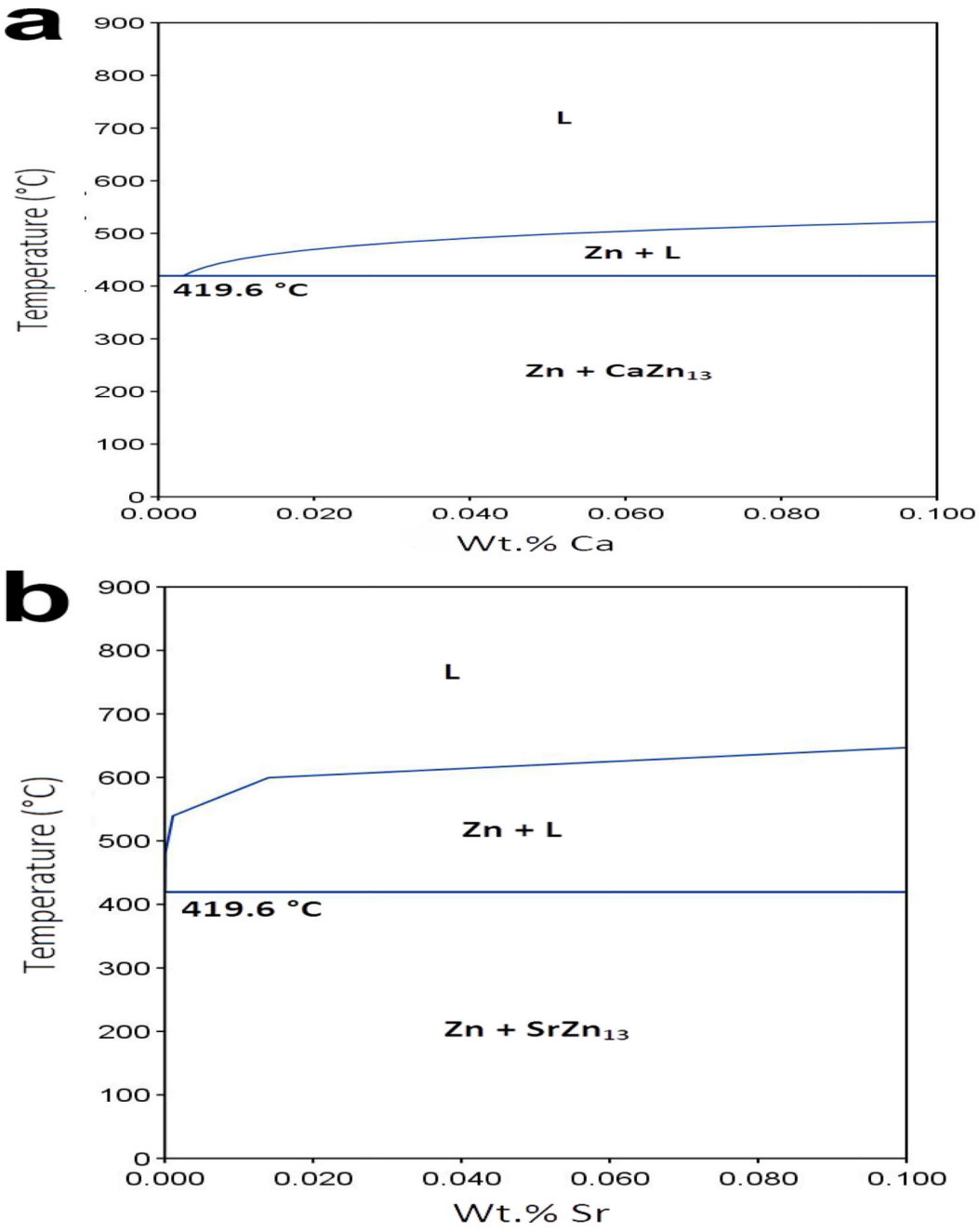

Fig. 8.

(a) Zn-Ca and (b) Zn-Sr equilibrium phase diagrams (based on Ref. [123]).

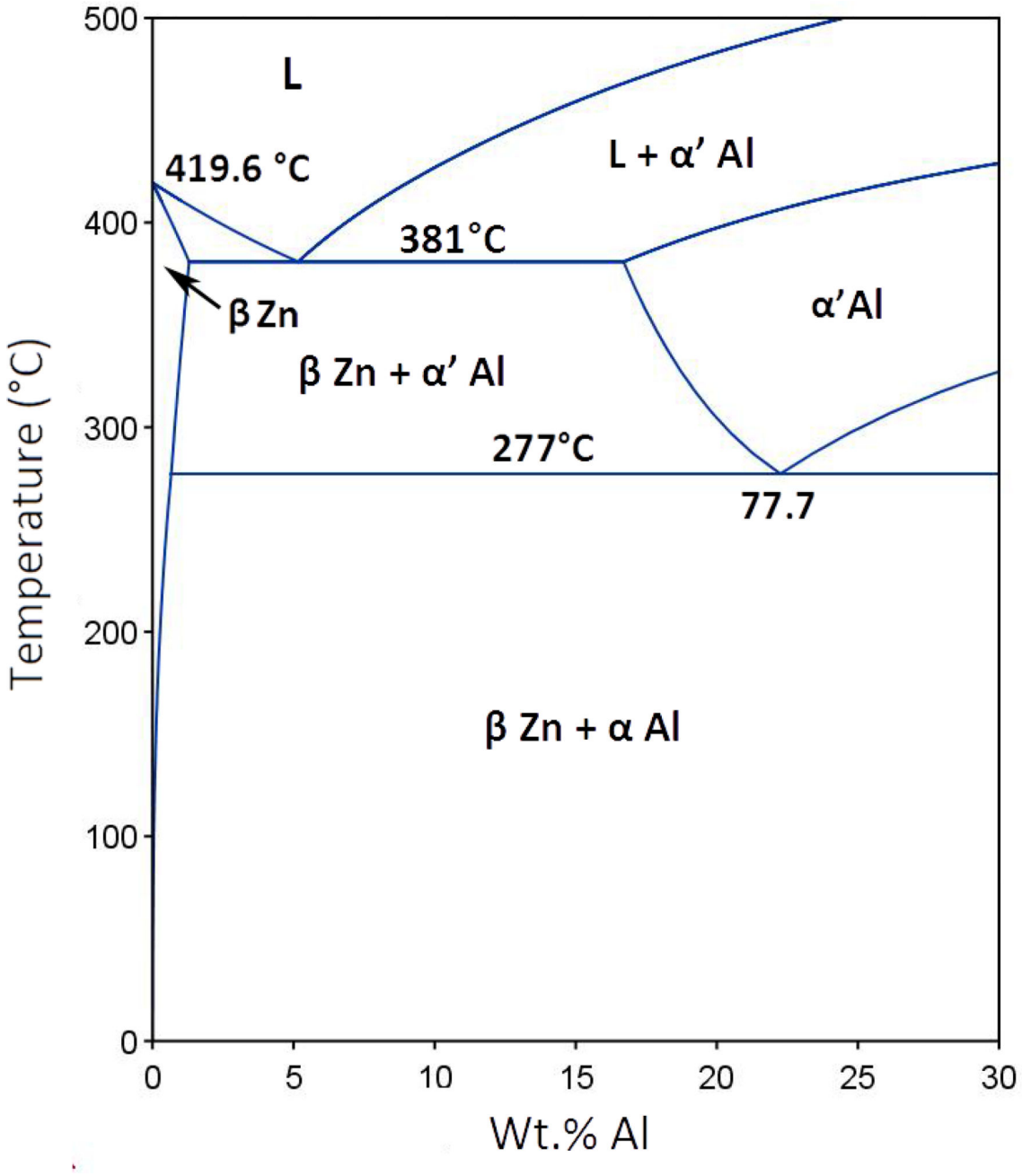

Fig. 9.
Zn-Al equilibrium phase diagram (based on Ref. [123]).

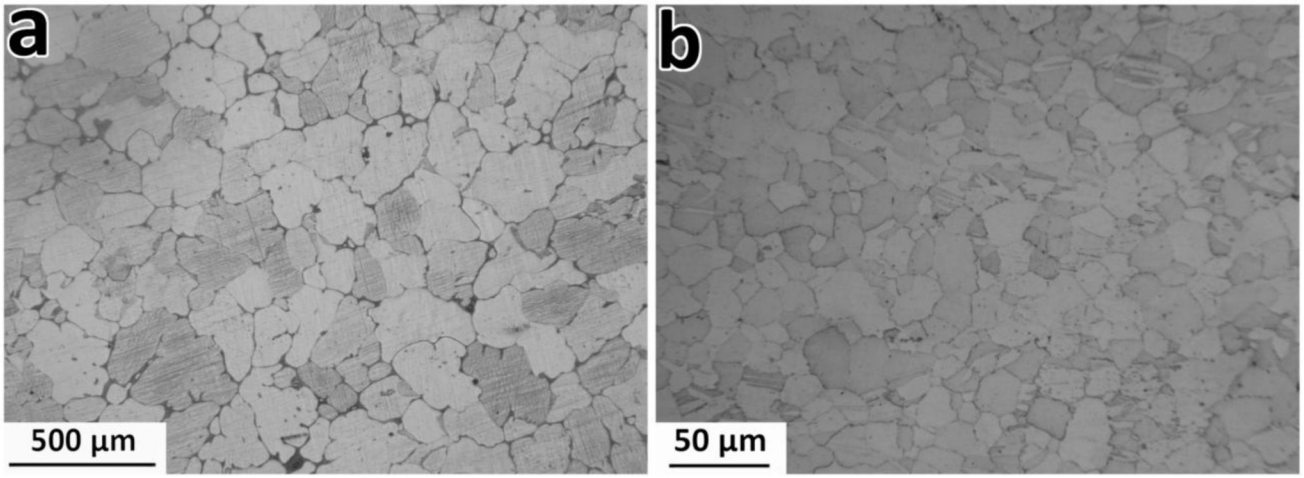

Fig. 10.
Microstructure of the (a) as-cast and (b) extruded Zn-1.0Al alloy.

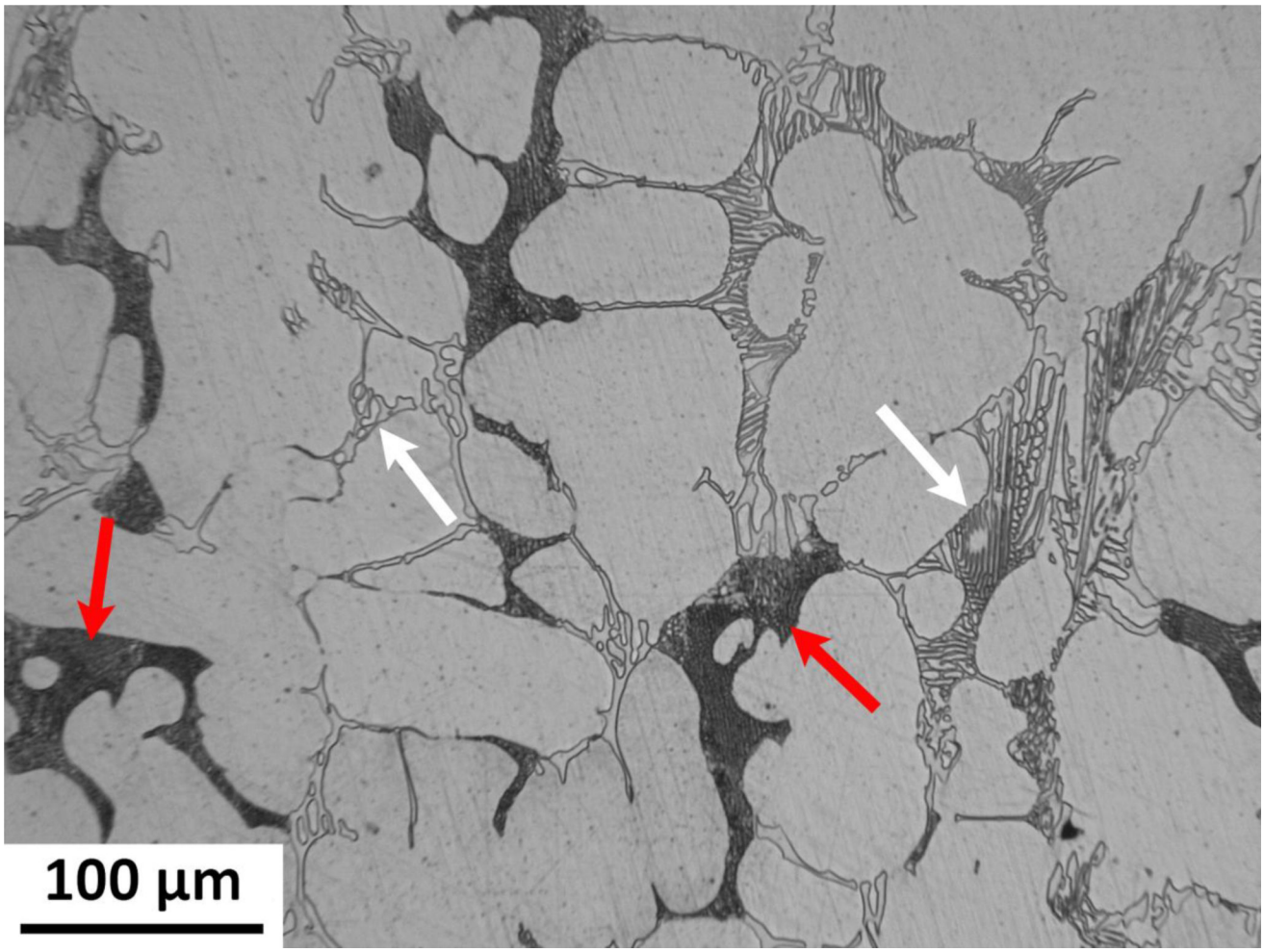

Fig. 11.
Microstructure of the as-cast Zn-1.0Al-1.0Mg alloy.

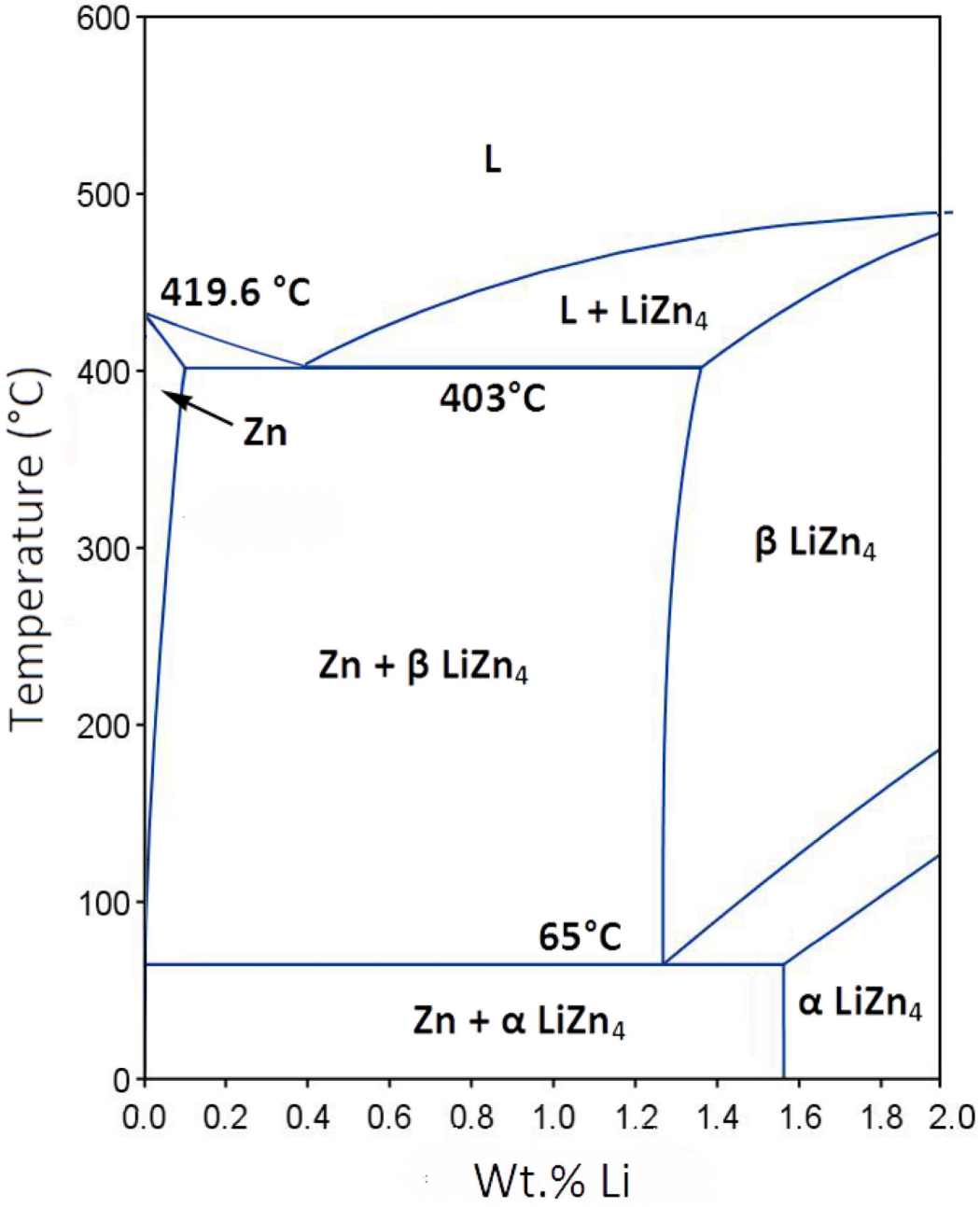

Fig. 12.
Zn-Li equilibrium phase diagram (based on Ref.[124]).

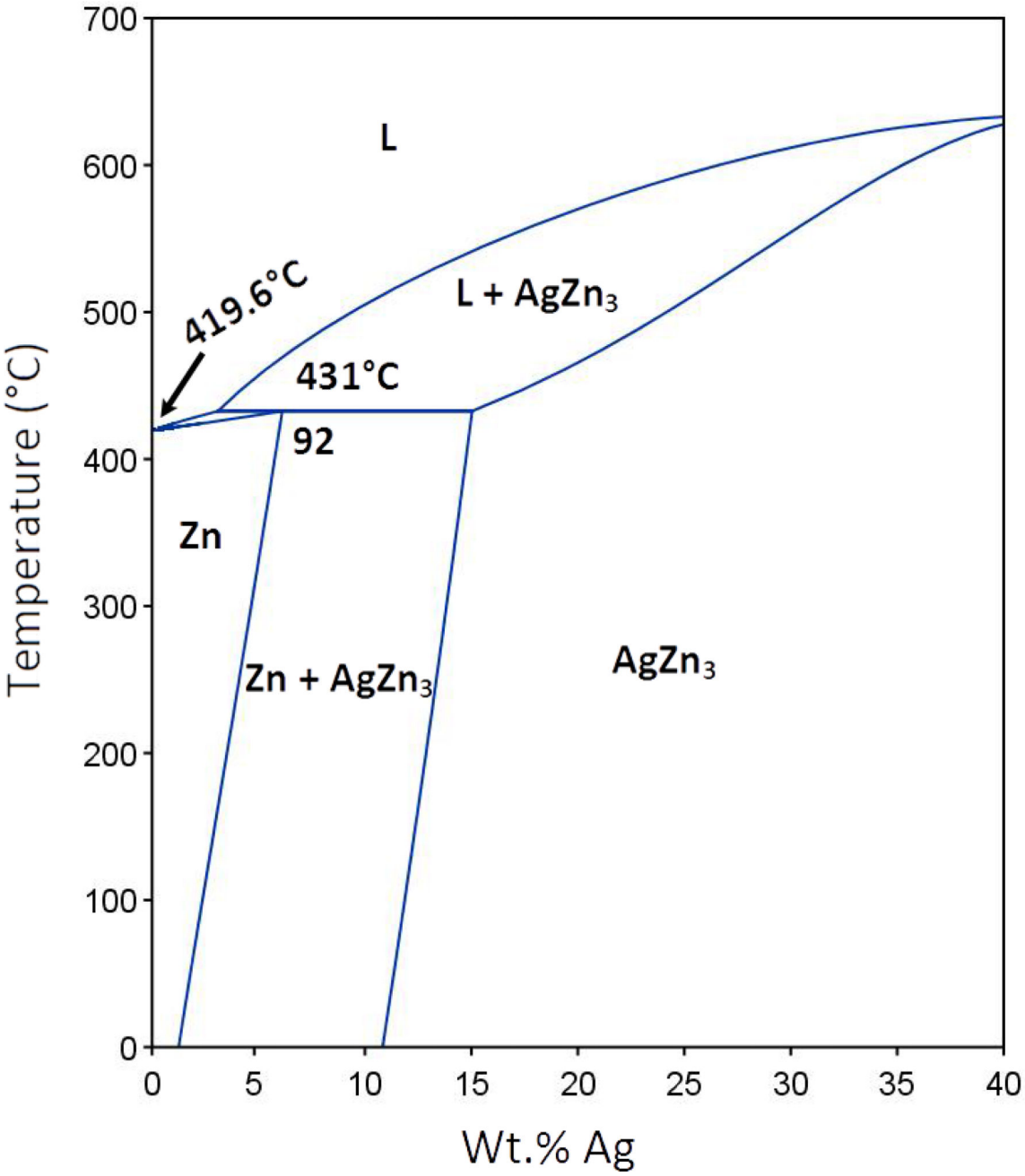

Fig. 13.
Zn-Ag equilibrium phase diagram (based on Ref. [123]).

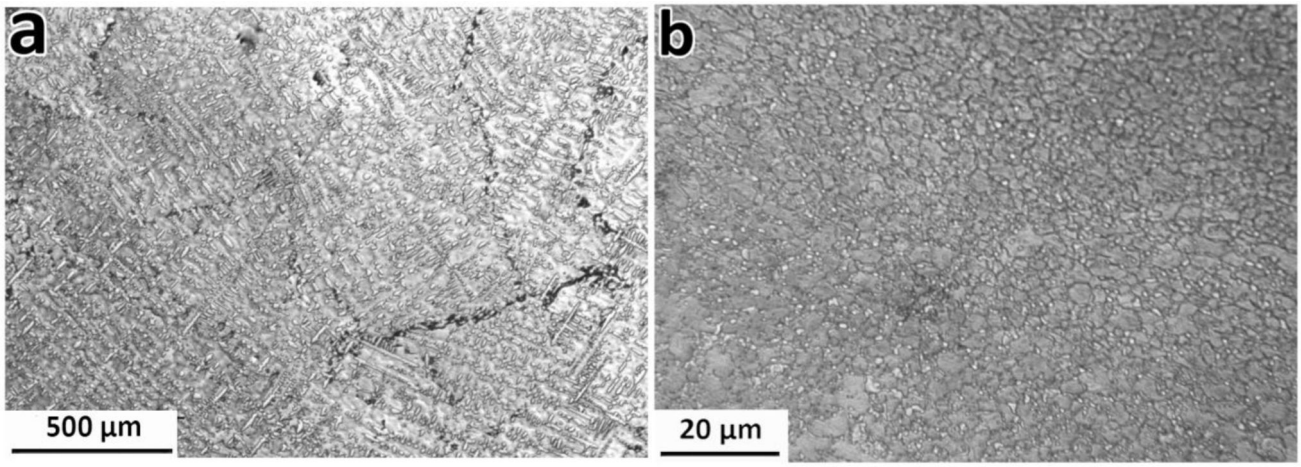

Fig. 14.
Microstructure of the (a) as-cast and (b) extruded Zn-7.0Ag alloy.

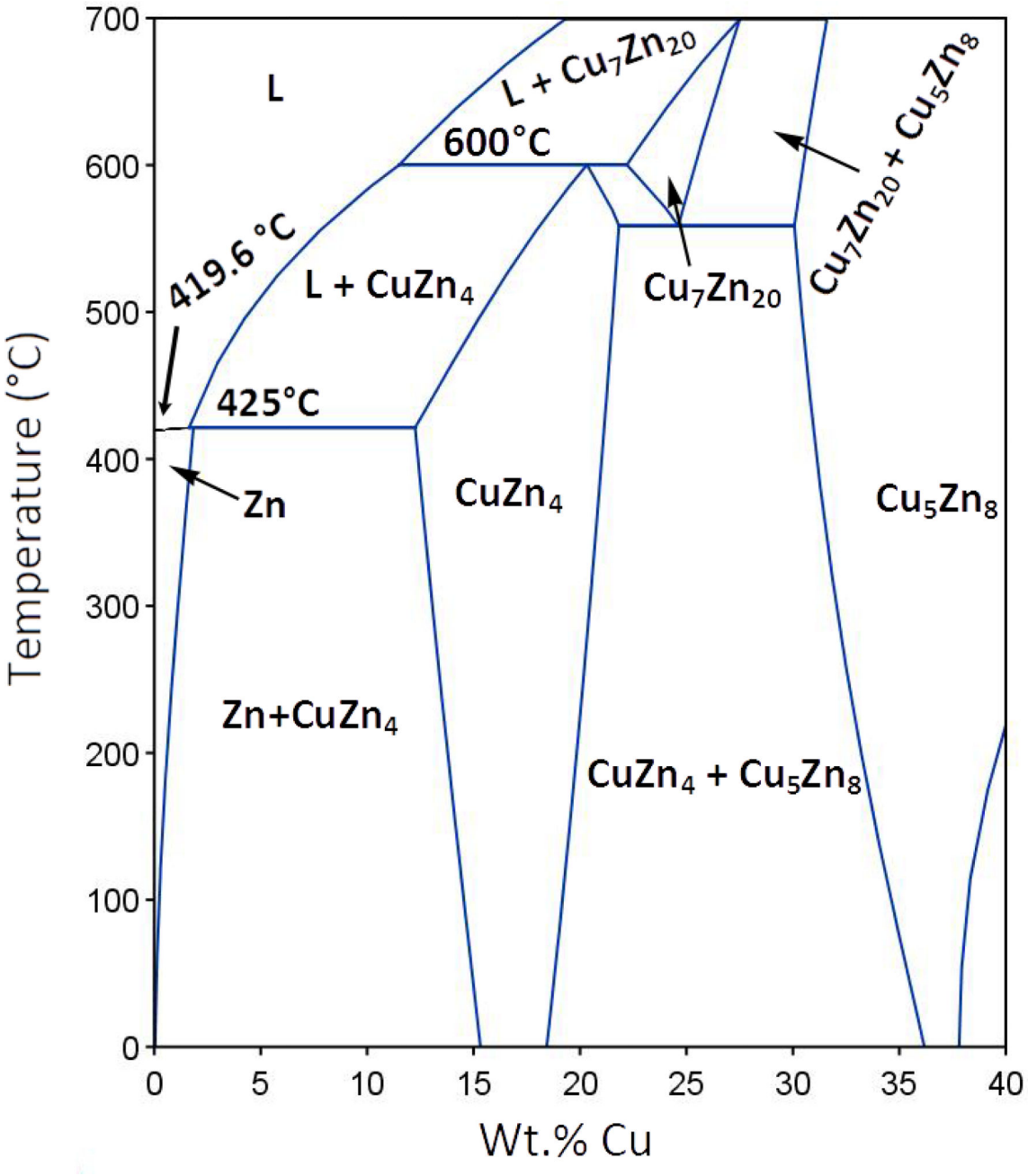

Fig. 15.
Zn-Cu equilibrium phase diagram (based on Ref. [123]).

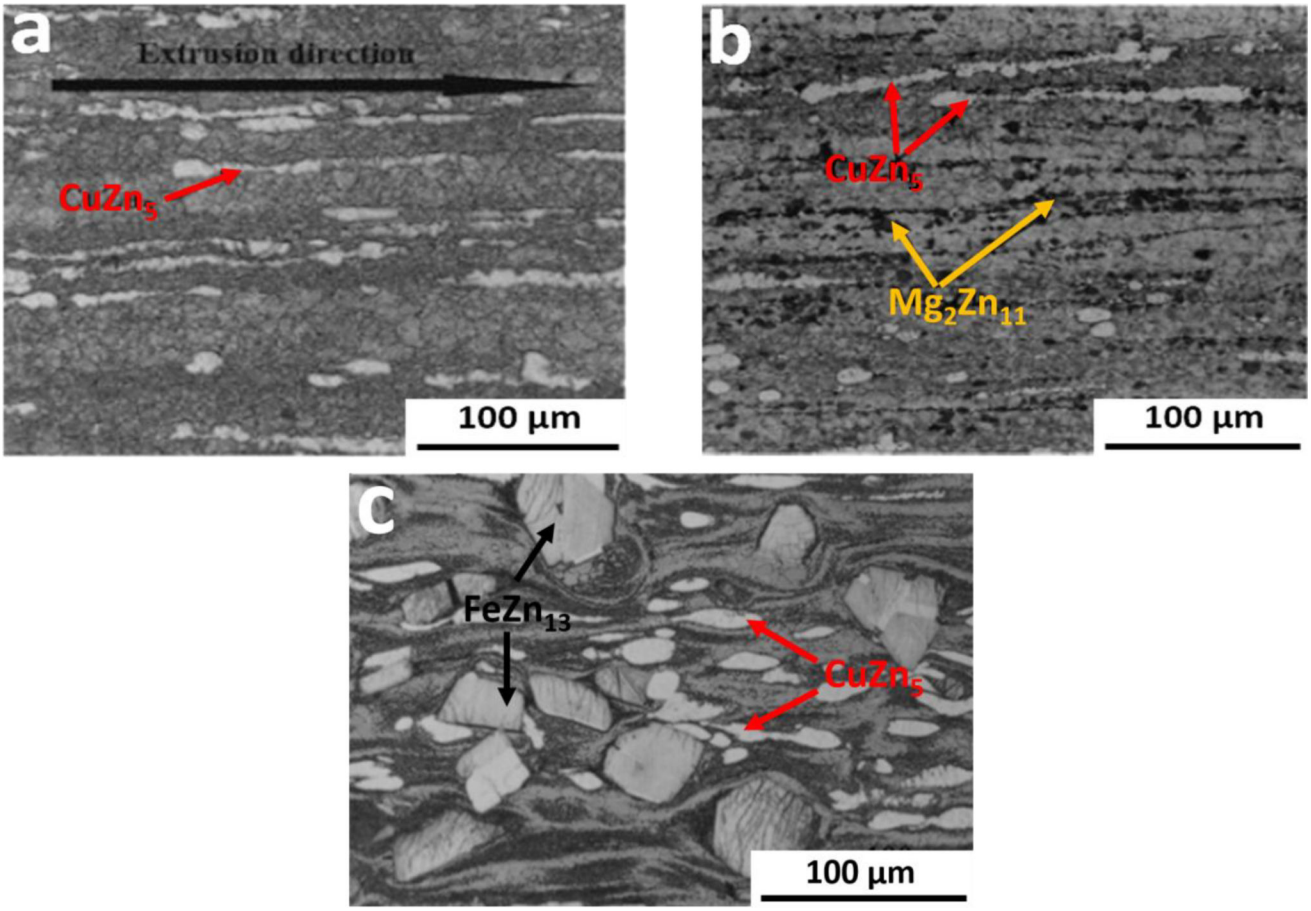

Fig. 16.

Microstructure of extruded (a) Zn-3Cu, (b) Zn-3Cu-0.5Mg and (c) Zn-3.0Cu-1.0Fe alloys. Reprinted with permission [100,101].

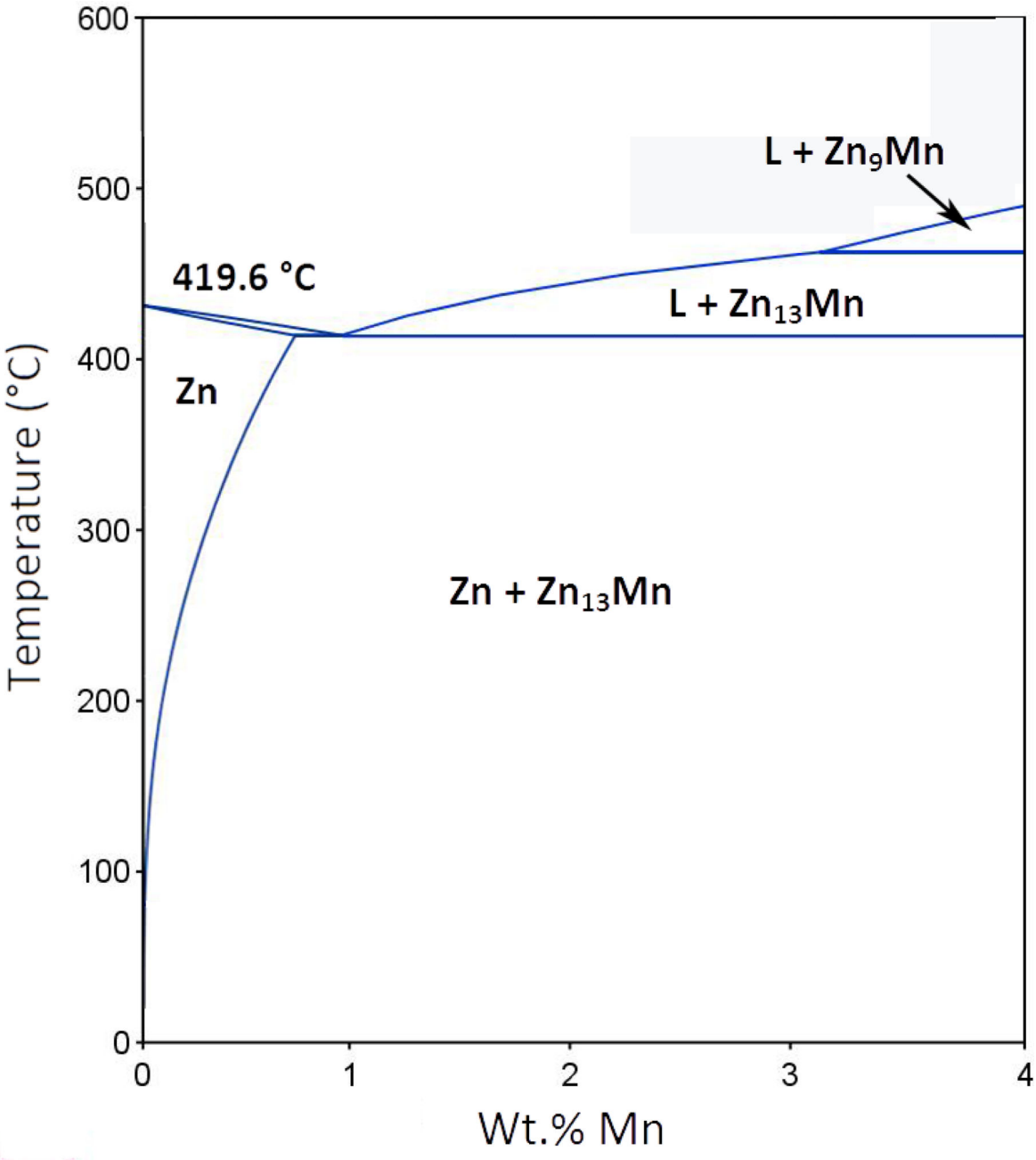

Fig. 17.
Zn-Mn equilibrium phase diagram (based on Ref. [123]).

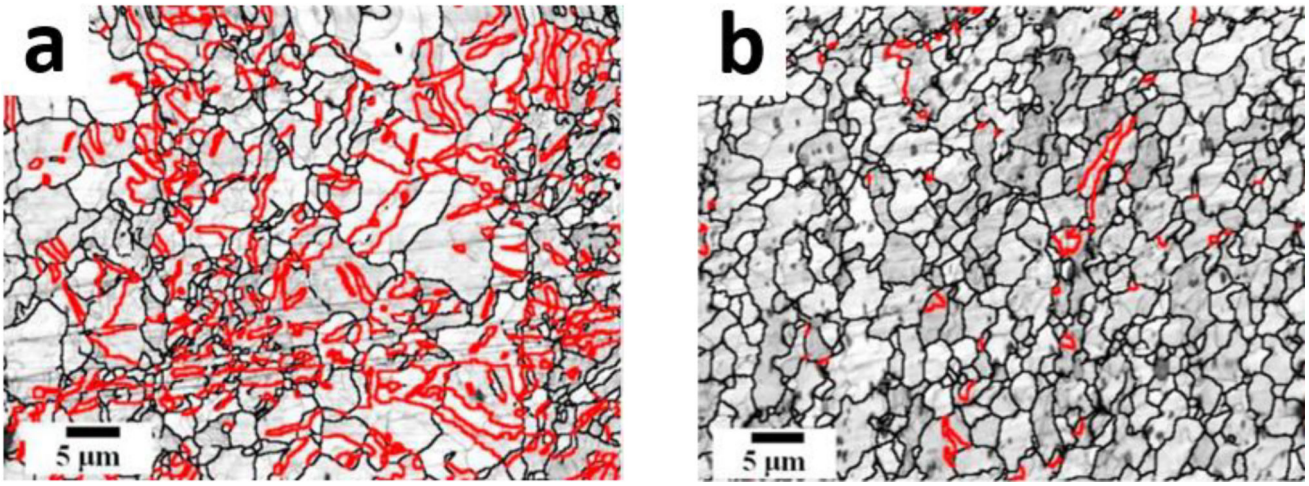

Fig. 18.

EBSD maps of as-extruded (a) Zn-0.2Mn and (b) Zn-0.6Mn alloys, highlighting the tensile twining in red. Reprinted with permission [103].

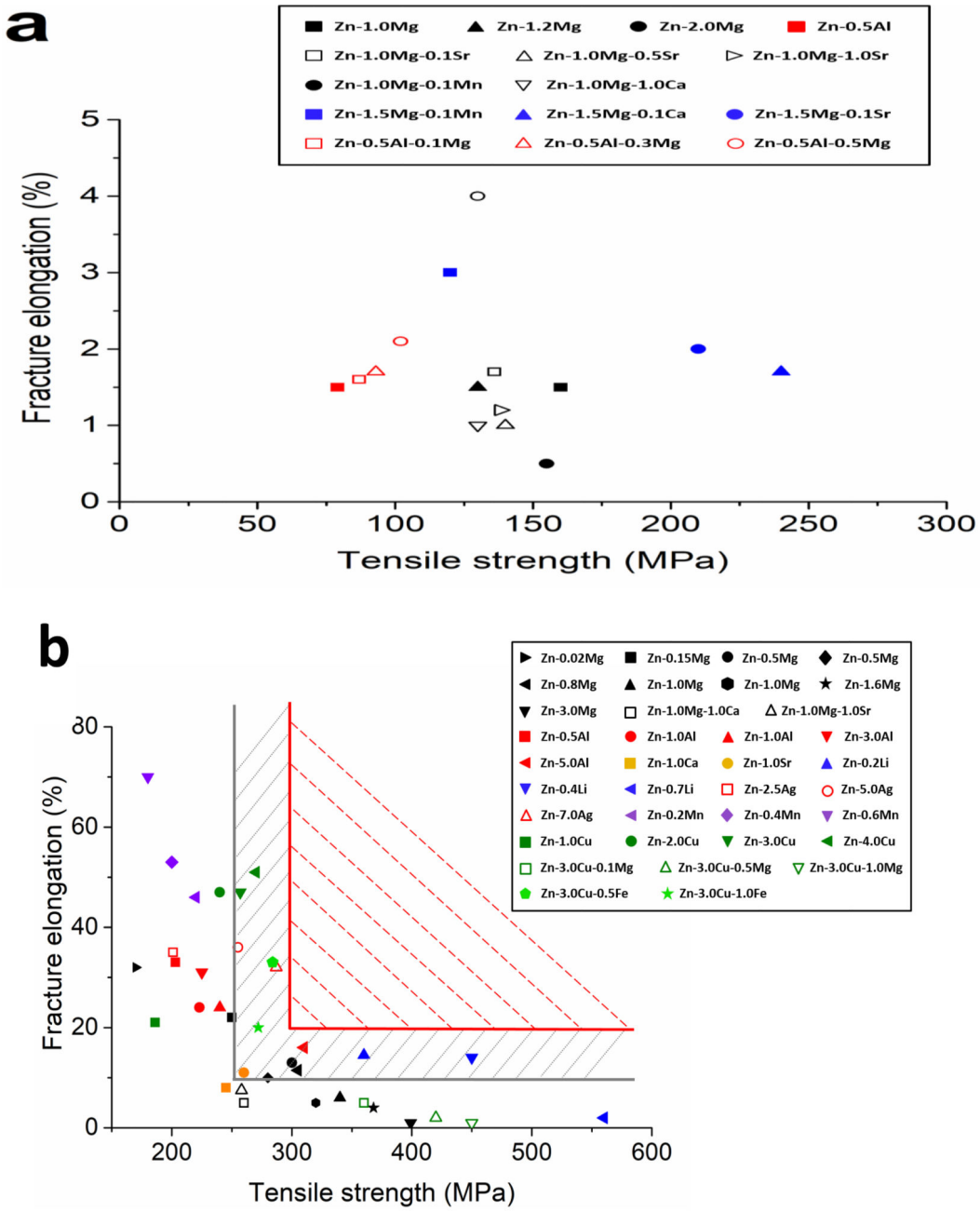

Fig. 19.

Fracture elongation versus ultimate tensile strength of (a) as-cast and (b) wrought Zn-based alloys (the red hachured region is where desirable materials could be placed, while alloys located in the grey hachured region are believed to be potential candidates for stent materials after further developments) [42–45,48–52,54,55,58,81,100,101,114,125].

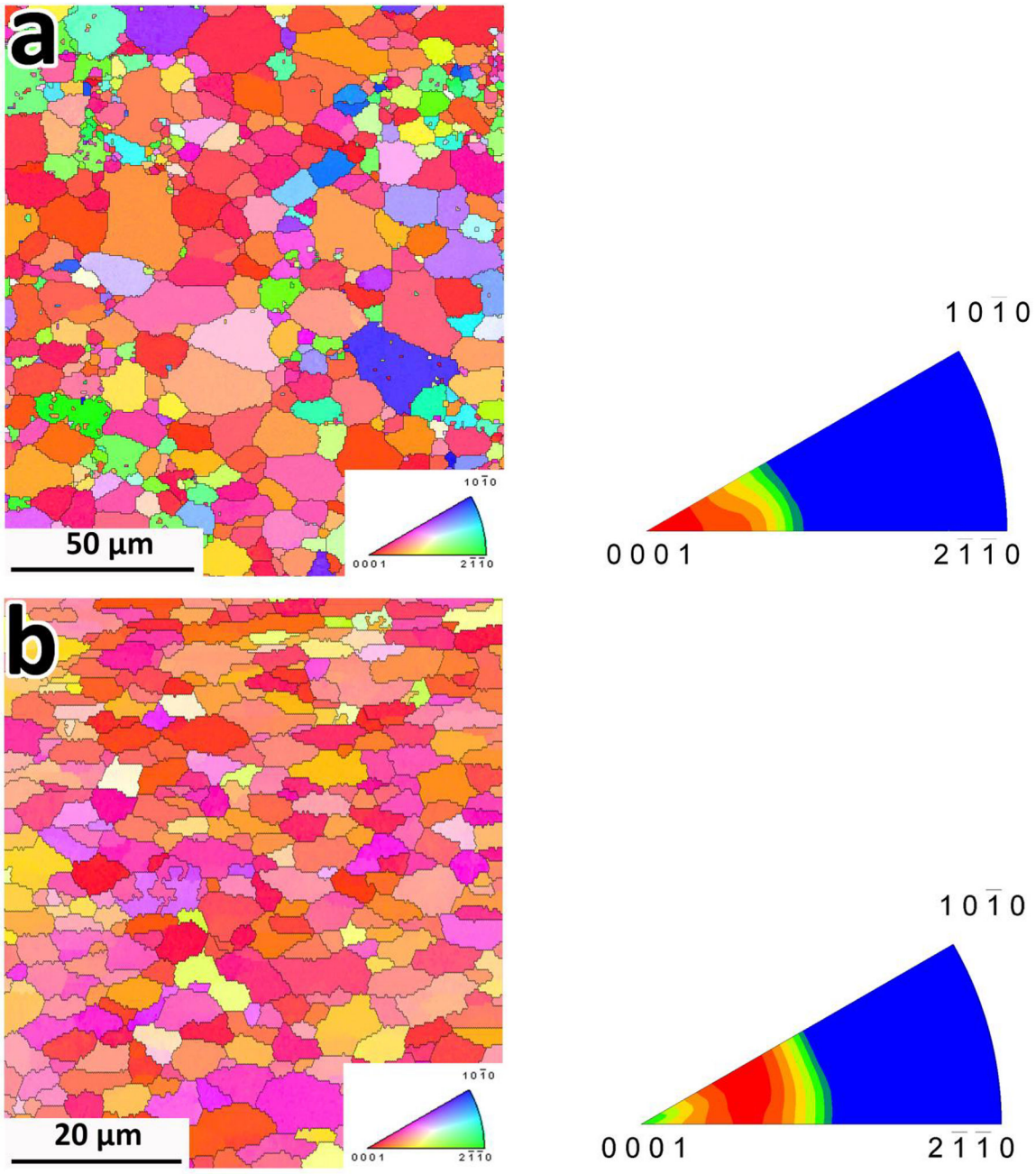

Fig. 20.

EBSD maps and the corresponding inverse pole figures of (a) ZK60 and (b) Zn-0.5Mg alloys. Reprinted with permission [43,116].

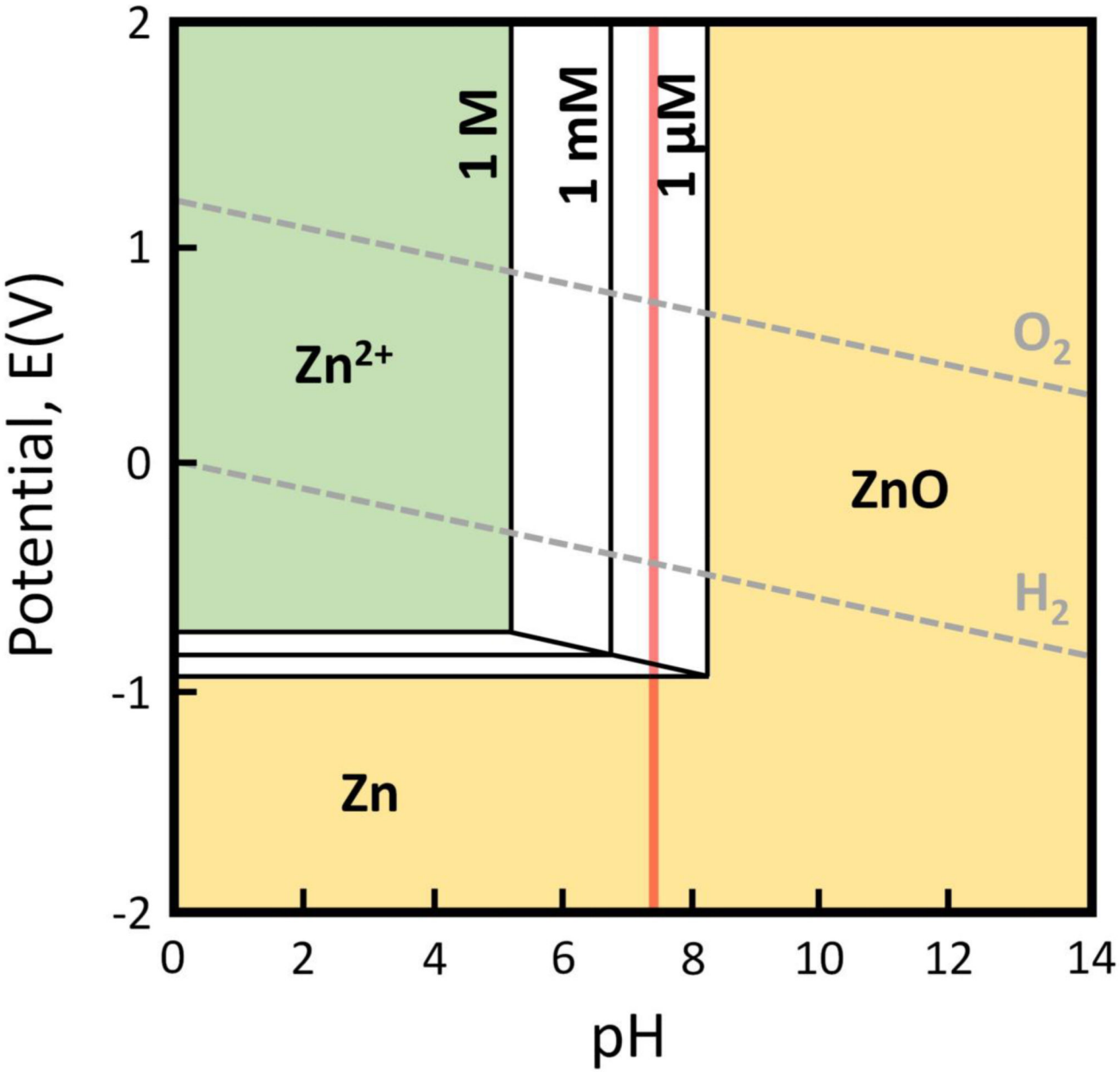

Fig. 21.

Pourbaix diagram for Zn in H_2O; (based on Ref. [7]). The region with aqueous species is colored green; concentration-dependent regions between $[Zn^{2+}]$ = 1 μ M and 1 M are in white; and solid species are shown in yellow. Physiological pH = 7.3 is shown by a red line.

Table 1

Summary of the *in vitro* corrosion studies for Zn and Zn-based biodegradable alloys.

Material		Corrosion rate (mm.year^{-1})		Solution	Other conditions	Time of immersion test (days)	Ref.
		Static immersion test	Potentiodynamic test				
Ultra-pure Zn plate		0.013	–	Hanks'	pH=7.4 R *=1/25	30	[53]
Ultra-pure Zn, laser cut tube		0.037					
Zn		–	0.03	DPBS	pH=7.4 agitation 80rpm	–	[118]
			0.10	Ringer'			
			0.19	Human plasma			
			0.11	Whole blood			
Zn	Cast & homogenized	0.061	–	aerated SBF	T=37°C pH=7	14	[42]
Zn-1Mg		0.075					
Zn-1.5Mg		0.069					
Zn-3Mg		0.073					
Zn-4Al-1Cu		0.078					
Zn-1Mg	As cast	0.28	–	SBF, renewed each 24 hours	T=37°C	7	[62]
	As extruded	0.12					
Zn-1.2Mg	As cast	0.07	0.12	Hanks'	T=37°C	90	[45]
	As extruded	0.09	0.19				
Zn-0.8 Mg	As extruded	0.071 (0.0134 mg.cm^{-2}.day^{-1})	–	DMEM, MEM	T=37°C agitation 125rpm	1	[114]
Zn-1.5Mg	As extruded	0.101 (0.019 mg.cm^{-2}.day^{-1})	–	DMEM, MEM	T=37°C pH= 7.4, 5% CO_2 atmosphere	3	[64]
Pure Zn	As rolled	0.078	0.135	Hanks'	T=37°C	14	[48]
Zn-1.0Mg		0.086	0.149				
Zn-1.0Ca		0.089	0.16				
Zn-1.0Sr		0.098	0.176				
Zn	As extruded	0.074	0.134	Modified Hanks' renewed each two days	T=37°C pH= 7.4 5% CO_2 atmosphere, 90% humidity	14	[43]
Zn-0.15Mg		0.078	0.164				

Material		Corrosion rate (mm.year^{-1})		Solution	Other conditions	Time of immersion test (days)	Ref.
		Static immersion test	Potentiodynamic test				
Zn-0.5Mg		0.082	0.164				
Zn-1.0Mg		0.084	0.169				
Zn-3.0Mg		0.076	0.128				
Zn-0.5Al		0.078	0.143				
Zn-1.0Al		0.079	0.145				
Zn	As extruded	0.075	0.135	Hanks’	T=37°C	56	[55]
Zn-1.0Mg-1.0Ca		0.090	0.169				
Zn-1.0Mg-1.0Sr		0.095	0.175				
Zn-1.0Ca-1.0Sr		0.011	0.187				
Zn	As cast	0.049	0.050	Hanks’	T=37°C pH=7.4 R=1/25	90	[51]
Zn-1.0Mg-0.1Mn	As cast	0.051	0.260				
	As rolled	0.070	0.140				
Zn-1.5Mg-0.1Mn	As cast	0.061	0.250				
Zn-1.5Mg	As cast	0.065	0.110	Hanks’	T=37°C pH=7.4 R=1/25	30	[54]
Zn-1.5Mg-0.1Ca		0.115	0.280				
Zn-1.5Mg-0.1Sr		0.105	0.106				
Zn-5.0Mg-1.0Fe	Rolled micro-tube	0.040	–	SBF	T=37°C	48	[65]
Zn-5.0Mg-1.0Fe	Drawn micro-tube	0.062					
Zn-4.0Cu	As extruded	0.0094	–	Hanks’ renewed each 24 hours	T=37°C R=1/25	20	[50]
Zn-1.0Cu	As extruded	0.033	–	SBF	T=37°C R=1/25	20	[106]
Zn-2.0Cu		0.026	–				
Zn-3.0Cu		0.030	–				
Zn-4.0Cu		0.025	–				
Zn-3.0Cu	As extruded	0.012	0.006	Hanks’	T=37°C R=1/25	20	[16]
Zn-3.0Cu-0.1Mg		0.022	0.018				
Zn-3.0Cu-0.5Mg		0.030	0.024				
Zn-3.0Cu-1.0Mg		0.043	0.185				

Material		Corrosion rate (mm.year^{-1})		Solution	Other conditions	Time of immersion test (days)	Ref.
		Static immersion test	Potentiodynamic test				
Zn-3.0Cu-0.5Fe	As extruded	0.064	0.104	SBF	T=37°C	20	[101]
Zn-3.0Cu-1.0Fe		0.069	0.131				
Zn	As extruded	0.077	0.133	Modified Hanks' renewed each two days	T=37°C, pH= 7.4 5% CO_2 atmosphere, 90% humidity	14	[44]
Zn-2.5Ag		0.079	0.137				
Zn-5.0Ag		0.081	0.144				
Zn-7.0Ag		0.084	0.147				
Zn	As rolled	–	0.160	SBF	T=37°C pH= 7.4 5% CO_2 atmosphere R =1/20	–	[81]
Zn-0.2Li			0.060				
Zn-0.4Li			0.050				
Zn	As extruded	–	0.027	Hanks'	–	–	[75]
ZA4-1			0.047				
ZA4-3			0.374				
ZA6-1			0.086				
Zn-0.5Al	As cast	0.080	–	SBF	–	30	[52]
Zn-0.5Al-0.1Mg		0.110					
Zn-0.5Al-0.3Mg		0.131					
Zn-0.5Al-0.5Mg		0.146					
Zn-0.5Al-0.5Mg	As cast	0.150	–	SBF	T=37°C pH= 7.6	30	[74]
Zn-0.5Al-0.5Mg-0.1Bi		0.170					
Zn-0.5Al-0.5Mg-0.3Bi		0.210					
Zn-0.5Al-0.5Mg-0.5Bi		0.280					

*R: ratio of surface area to solution volume in (cm^2/ml)

Table 2

Summary of the *in vitro* studies on biocompatibility of Zn and Zn-based biodegradable alloys.

Cell line	Material	Major findings	Ref
Human dermalfibroblasts (hDF), Human aortic smooth muscle cells(AoSMC), Human aortic endothelial cells (HAEC)	Pure Zn	HAEC exhibited superior tolerance for Zn^{2+} (LD_{50}~265μM), while the viabilities of hDF (LD_{50}~50μM) and AoSMC (LD_{50}~70μM) decreased significantly with increasing concentration of Zn^{2+} ions. Direct culture revealed negligible cell survival on the Zn surface	[107]
MC3T3-E1 mouse osteoblast	Zn-Al-Mg Zn-Al-Mg-Bi	Increase in the viability of MC3T3-E1 cells for Zn extracts compared to the control group was observed. Addition of Bi from 0.1 to 0.5 wt% to the ternary alloy reduced the viability of MC3T3-E1 compared to Zn-Al-Mg and negative control group due to the higher degradation rate of the Bi containing alloy.	[74]
Murine fibroblasts L929 Human osteosarcoma cells U-2 OS	Zn-0.8Mg	Zn is less biocompatible than Mg. The maximum safe concentrations of Zn^{2+} for the U-2 OS and L929 cells are 120 μM and 80 μM, respectively. Genotoxicity and mutagenicity tests did not reveal any negative effects related to Zn.	[114]
The human endothelial cell line EA.hy926	Zn-Cu Zn-Cu-Mg	In case of binary alloys, for 10% and 50% diluted extracts, the cell viability was always close to 100% at each culture time. The cells cultured in 100% extract show lower viability (10 – 20% of the control). 100% extracts of Zn-Cu-Mg alloys met the cytotoxicity standards. Enhanced cells viability of ternary alloys was attributed to the presence of Mg.	[100] [106]
Murine fibroblasts L929 Human osteosarcoma cells U-2 OS	Zn-1.5Mg	Test was performed on untreated and pre-incubated samples. The pre-incubated samples revealed higher – above 70% metabolic activity of L929 cells. U-2 OS cells were used in direct tests. Osteoblast-like cell growth directly on the samples was observed.	[64]
Human osteosarcoma cells lines: HOS and MG63 cells	Zn-1.2Mg	Cells cultured in the extraction medium at concentrations of 100%, 75%, 50%, 25% and 12.5% for 3 days. For HOS cells, a higher extract concentration reduced cell viability and induced cytotoxicity (cell viability below 10%). For MG63 cells high extract concentrations showed a slightly reduced cell viability. Extracts of 50% and 25% contributed to an increase of cytocompatibility, which exceeded 100% of the negative control group. It was suggested that a certain level of Zn^{2+} ions might promote cell attachment and proliferation, resulting in increases in bone healing and new bone formation.	[48]
Human osteosarcoma cells (MG63), human umbilical vein endothelial cells (ECV304) Rodent vascular smooth muscle cells (VSMC)	Pure Zn and Zn-1X alloys where X= Mg, Sr, Ca	For ECV304 cell, the Zn-1X alloys revealed high cell viabilities compared to pure Zn. For VSMC cell, the alloying elements do not have major influence on cells viability. For MG63, extracts of pure Zn lead to reduced cell viability compared to negative controls. Addition of the alloying elements Mg, Ca and Sr into Zn increased the viability of and promoted MG63 cell proliferation.	[45]
NHOst primary cells	Zn-3.0Mg	When the NHOst cells were exposed to Zn-containing extracts, their viability was reduced 30–50% of the control, because of the high concentration of Zn^{2+} in the extract (8μM). When compared to pure Zn, lower inhibitory effect of Zn–3Mg on the cells was attributed to an alloying with Mg resulting in lower corrosion rate.	[110]
Primary human coronary artery endothelial cells (HCECs)	Zn^{2+} containing solution	The study confirmed that cellular responses depend on the concentration of Zn^{2+} ions. At low concentrations, Zn^{2+} enhanced cell viability, proliferation, adhesion, spreading and migration. Further, it affected cell morphology; elongated shapes were observed in case of low ion concentrations. Nevertheless, cell adhesion strength was reduced. In contrast, high Zn^{2+} concentrations were observed to have detrimental effect on HCECs behavior.	[108]
Human mesenchymal stem cell (hMSC) derived from bone marrow	Pure Zn	Zn supports hMSC adhesion and proliferation. Mineralization of ECM and hMSC osteogenic differentiation were noticeably improved, featuring increased expression of bone-related genes (such as ALP, collagen I, and osteopontin). Finally, the presence of	[109]

Cell line	Material	Major findings	Ref
		Zn^{2+} lead to enhanced regulation of genes, cell survival growth and differentiation, ECM mineralization, and osteogenesis.	

Table 3

Summary of the *in vivo* tests for Zn and Zn-based biodegradable alloys.

Material	Animal model	Duration (months)	Findings	Degradation rate ($mm \cdot year^{-1}$)	Ref.
Zn wire, 99.99% purity	Abdominal aorta of Sprague-Dawley rats	1.5 3.0 4.5 6.0	Critical aspects of biocorrosion – the rate of penetration and the immediate effects of generated products satisfy the requirements for stent application; Zn wire remained intact for 4 months; followed by acceleration of the corrosion; corrosion products on zinc after 4.5 and 6 months were mainly made of ZnO and $ZnCO_3$.	After X months (X= 1.5, 3.0, 4.5, 6.0) 1.5 = 0.012 3.0 = 0.02 4.5 = 0.042 6.0 = 0.048	[8]
Zn wire, 99.99% purity		2.5 6.5	Excellent biocompatibility with arterial tissues, no inflammatory response and no progressive intimal hyperplasia	-	[112]
Zn wires: - 99.99% purity - electropolished - oxidized - anodized		1.0 2.0 3.0	Zn corrosion rate varied with different surface engineering of thin oxide films; degradation rate depended on the quality and stability of the oxide film; electropolished and anodized wires corroded slower than untreated ones.	-	[40]
Zn-Li extruded wires		2.0 4.0 6.5 9.0 12.0	Zn-Li retained about 70% of its original dimension after 12 months follow up; alloy exhibited nearly linear relationship between the percent of area reduction and time; ideal uniform gradual acceleration of biodegradation; moderate inflammation with non-obstructive neointima.	After X months (X=2, 4, 6.5, 9, 12) 2.0 = 0.007 4.0 = 0.015 6.5 = 0.020 9.0 = 0.037 12.0 = 0.045	[47]
Zn-xAl rolled strips (x=1, 3, 5)		1.5 3.0 4.5 6.0	Zn-Al showed acceptable compatibility with surrounding arterial tissue; no necrotic tissue was detected; indications of chronic and acute inflammation were observed; biocorrosion rates were higher at initial stages than that of pure Zn.	-	[49]

Material	Animal model	Duration (months)	Findings	Degradation rate (mm·year^{-1})	Ref.
Zn-xMg wires (x=0.002; 0.005; 0.08)		1.5 3.0 4.5 6.0 11.0	Zn-Mg alloys featured uniform degradation mode. The increase in degradation rates in later stages of implantation was detected. Slightly decrease in biocompatibility with increasing Mg content was observed. This effect was attributed to the improved corrosion resistance of Zn-0.08Mg alloy. Further, it was confirmed that corrosion resistant Mg_2Zn_{11} intermetallic phase stimulates a more aggressive activity of macrophages.	After X months (X=1.5; 3; 4.5; 6; 11), Zn-0.002Mg vs Zn-0.08Mg 1.5 = 0.029 vs 0.012 3.0 = 0.021 vs 0.013 4.5 = 0.026 vs 0.015 6.0 = 0.032 vs 0.027 11.0 = 0.051 vs 0.023	[59]
Electropolished Zn stents (Φ3.0 × 10 mm, strut thickness 165 μm)	Abdominal aortas of adult Japanese rabbits	1.0 3.0 6.0 12.0	Pure zinc implants preserved their mechanical integrity for 6 months. Dissolution of 41.75 ± 29.72% of the stent's volume after 12 months of implantation was observed. No severe inflammation, platelet aggregation, thrombosis formation or obvious intimal hyperplasia was observed.	After X months (X=1; 3; 6; 12): 1.0 = 0.03 3.0 = 0.01 6.0 = 0.01 12.0 = 0.02	[113]